NASA/TM—2003-211983

Basic Equations for the Modeling of Gallium Nitride (GaN) High Electron Mobility Transistors (HEMTs)

Jon C. Freeman
Glenn Research Center, Cleveland, Ohio

February 2003

The NASA STI Program Office . . . in Profile

Since its founding, NASA has been dedicated to the advancement of aeronautics and space science. The NASA Scientific and Technical Information (STI) Program Office plays a key part in helping NASA maintain this important role.

The NASA STI Program Office is operated by Langley Research Center, the Lead Center for NASA's scientific and technical information. The NASA STI Program Office provides access to the NASA STI Database, the largest collection of aeronautical and space science STI in the world. The Program Office is also NASA's institutional mechanism for disseminating the results of its research and development activities. These results are published by NASA in the NASA STI Report Series, which includes the following report types:

- TECHNICAL PUBLICATION. Reports of completed research or a major significant phase of research that present the results of NASA programs and include extensive data or theoretical analysis. Includes compilations of significant scientific and technical data and information deemed to be of continuing reference value. NASA's counterpart of peer-reviewed formal professional papers but has less stringent limitations on manuscript length and extent of graphic presentations.

- TECHNICAL MEMORANDUM. Scientific and technical findings that are preliminary or of specialized interest, e.g., quick release reports, working papers, and bibliographies that contain minimal annotation. Does not contain extensive analysis.

- CONTRACTOR REPORT. Scientific and technical findings by NASA-sponsored contractors and grantees.

- CONFERENCE PUBLICATION. Collected papers from scientific and technical conferences, symposia, seminars, or other meetings sponsored or cosponsored by NASA.

- SPECIAL PUBLICATION. Scientific, technical, or historical information from NASA programs, projects, and missions, often concerned with subjects having substantial public interest.

- TECHNICAL TRANSLATION. English-language translations of foreign scientific and technical material pertinent to NASA's mission.

Specialized services that complement the STI Program Office's diverse offerings include creating custom thesauri, building customized databases, organizing and publishing research results . . . even providing videos.

For more information about the NASA STI Program Office, see the following:

- Access the NASA STI Program Home Page at ***http://www.sti.nasa.gov***

- E-mail your question via the Internet to help@sti.nasa.gov

- Fax your question to the NASA Access Help Desk at 301–621–0134

- Telephone the NASA Access Help Desk at 301–621–0390

- Write to:
  NASA Access Help Desk
  NASA Center for AeroSpace Information
  7121 Standard Drive
  Hanover, MD 21076

NASA/TM—2003-211983

Basic Equations for the Modeling of Gallium Nitride (GaN) High Electron Mobility Transistors (HEMTs)

Jon C. Freeman
Glenn Research Center, Cleveland, Ohio

National Aeronautics and
Space Administration

Glenn Research Center

February 2003

Available from

NASA Center for Aerospace Information
7121 Standard Drive
Hanover, MD 21076

National Technical Information Service
5285 Port Royal Road
Springfield, VA 22100

Available electronically at http://gltrs.grc.nasa.gov

Basic Equations for the Modeling of Gallium Nitride (GaN) High Electron Mobility Transistors (HEMTs)

Jon C. Freeman
National Aeronautics and Space Administration
Glenn Research Center
Cleveland, Ohio 44135

Summary

Gallium nitride (GaN) is a most promising wide band-gap semiconductor for use in high-power microwave devices. It has functioned at 320 °C, and higher values are well within theoretical limits. By combining four devices, 20 W has been developed at X-band. GaN High Electron Mobility Transistors (HEMTs) are unique in that the two-dimensional electron gas (2DEG) is supported not by intentional doping, but instead by polarization charge developed at the interface between the bulk GaN region and the AlGaN epitaxial layer. The polarization charge is composed of two parts: spontaneous and piezoelectric. This behavior is unlike other semiconductors, and for that reason, no commercially available modeling software exists. The theme of this document is to develop a self-consistent approach to developing the pertinent equations to be solved. A Space Act Agreement, "Effects in AlGaN/GaN HEMT Semiconductors" with Silvaco Data Systems to implement this approach into their existing software for III-V semiconductors, is in place (summer of 2002).

Introduction

This report describes a method to model gallium nitride (GaN) with the Silvaco product ATLAS and its subroutine BLAZE. Unlike other semiconductor systems, GaN requires the addition of strains at all parts of the device to include the effects of piezoelectricity. One must also include a spontaneous polarization at certain interfaces. For these reasons this report consists of 11 sections. Section 1 introduces notations and definitions, in the area of linear elasticity. Section 2 discusses piezoelectricity and gives the complete set of basic equations to be solved in a general GaN device. Section 3 introduces spontaneous polarization. Section 4 indicates the additions needed in the Poisson-Schrodinger solver for GaN analysis. Section 5 gives some critical and basic details on the layer structure of AlGaN/GaN HEMTs. Section 6 covers band-gap variations, while the remaining sections treat necessary issues to complete the analysis.

Discussion

Our goal is to model AlGaN/GaN HEMTs using Silvaco's existing software platform. For the AlGaN/GaN system and other III-V nitrides, the effects of both spontaneous and piezoelectric polarization fields must be included in an analysis. These fields dominate the properties of the 2DEG, and this report serves as a starting point to incorporate them. The polarizations enter the problem via the constitutive equation relating $\overline{D}, \overline{E}$, and $\overline{P}$:

$$\overline{D} = \epsilon_0 \epsilon_r \overline{E} + \overline{P}$$

Where $\overline{D}$ is the electric flux density, $\overline{E}$ the electric field, and $\overline{P}$ the polarization of the material. This then influences Poisson's equation as follows. Taking the divergence of the previous equation we have

$$\nabla \cdot \overline{D} = \epsilon_o \epsilon_r \nabla \cdot \overline{E} + \nabla \cdot \overline{P}$$

Then Poisson's equation is

$$\nabla \cdot \overline{D} = \rho$$

or

$$\epsilon_o \epsilon_r \left(\nabla \cdot \left(-\nabla \phi\right)\right) + \nabla \cdot \overline{P} = \rho$$

$$-\epsilon_o \epsilon_r \nabla^2 \phi = \rho - \nabla \cdot \overline{P}$$

Thus the form using the electrostatic potential has an "extra" term due to polarizations not included in the relative dielectric constant ϵ_r. The added polarization $\overline{P}$ is composed of both the spontaneous and piezoelectric parts. The spontaneous part is modeled with an ab initio result of a theoretical calculation, while the piezoelectric portion must be determined from the stress/strain fields of the device. The constitutive equations for the stress/strain and $\overline{D}, \overline{E}$, and $\overline{P}$ are:

$$\overleftrightarrow{S} = d_T \cdot \overline{E} + S^E : \overleftrightarrow{T}$$

$$\overline{D} = \kappa^S \cdot \overline{E} + d : \overleftrightarrow{T} \Rightarrow \overline{P} = d : \overleftrightarrow{T}$$

The quantities $\overleftrightarrow{T}, \overleftrightarrow{S}, S^E, d, \kappa^S$, are the stress, strain, compliance, piezoelectric, and permittivity tensors, respectively.

The fact that $\overline{P}$ modifies Poisson's equation means that it also modifies the energy levels for the 2DEG as obtained from the Schrodinger equation. The strain also modifies the band gaps, via the deformation potential terms.

This report consists of eleven sections. Section 1 introduces notations in the area of linear elasticity. Section 2 discusses piezoelectricity. Section 3 treats the concepts and properties of spontaneous polarization, as this is a dominant term, yet it is not well understood. Section 4 develops the forms for Poisson's and Schrodinger's equations. Here, the inclusion of dipoles and dangling bonds at the interface is addressed. Section 5 gives an account of the issues concerning the stresses and strains in AlGaN/GaN systems. Section 6 discusses the very important band-gap issues. Section 7 is just one page covering the variation in thermal conductivity with temperature. Section 8 gives numerical values for many of the terms discussed in other sections. It shows that the polarization terms are indeed dominant, as shown in published works. The effects of residual strains, strains due to interface mismatch, and oxide and metal pads are covered. Section 9 briefly visits some of the issues concerning heterojunctions. Section 10 gives data on many of the known traps discussed in the open literature. Finally, section 11 is a discussion of amplifiers and the best power levels reported to date. The appendix gives the closed-form expression for the field due to the spontaneous polarization.

1. Elasticity

This section serves to introduce the needed definitions in elasticity theory that will be utilized later. Let u = mechanical displacement, then the strain is defined as (ref. 1)

$$\bar{S}_{ij}(\bar{r},t)=\frac{1}{2}\left(\frac{\partial u_i}{\partial r_j}+\frac{\partial u_j}{\partial r_i}\right) \quad i,j=x,y,z \tag{1}$$

where S_{ij} means i = direction of displacement (or force)
j = normal to surface (face)

Strain is commonly given the symbols $\in_{xx}$, u_{xx}, . . .
Now

$$\overleftrightarrow{S}=\begin{bmatrix} S_{xx} & S_{xy} & S_{xz} \\ S_{xy} & S_{yy} & S_{yz} \\ S_{xz} & S_{yz} & S_{zz} \end{bmatrix} \underline{\underline{\Delta}} \begin{bmatrix} S_1 & \frac{1}{2}S_6 & \frac{1}{2}S_5 \\ \frac{1}{2}S_6 & S_2 & \frac{1}{2}S_4 \\ \frac{1}{2}S_5 & \frac{1}{2}S_4 & S_3 \end{bmatrix} \tag{2}$$

Following Auld (ref. 1), Nye (ref. 2), and many others, we use the convention that compressive strain is negative, while tensile is positive. Note that the factors of ½ and sign convention vary in the literature. Write

$$\overleftrightarrow{S}=\begin{bmatrix} S_1 \\ S_2 \\ S_3 \\ S_4 \\ S_5 \\ S_6 \end{bmatrix} \tag{3}$$

The stress is given as

$$\overleftrightarrow{T}=\begin{bmatrix} T_{xx} & T_{xy} & T_{xz} \\ T_{xy} & T_{yy} & T_{yz} \\ T_{xz} & T_{yz} & T_{zz} \end{bmatrix}=\begin{bmatrix} T_1 & T_6 & T_5 \\ T_6 & T_2 & T_4 \\ T_5 & T_4 & T_3 \end{bmatrix} \tag{4}$$

Alternate symbols for T_j are σ_{xx}, τ_{xy}, . . .

Write

$$\overleftrightarrow{T} = \begin{bmatrix} T_1 \\ T_2 \\ T_3 \\ T_4 \\ T_5 \\ T_6 \end{bmatrix} \qquad \begin{array}{l} T_j < 0 \text{ for compression} \\ T_i > 0 \text{ for tension} \end{array} \tag{5}$$

Assume linear theory is applicable, then Hooke's law is valid, so

$$T_{ij} = c_{ijkl} S_{kl} \tag{6}$$

or

$$S_{ijkl} = s_{ijkl} T_{kl} \tag{7}$$

where c_{ijkl} are the stiffness constants (N/m^2) and s_{ijkl} are the compliance constants (m^2/N).

The compact notation is

$$\overleftrightarrow{T} = \overline{\overline{c}} : \overleftrightarrow{S} \tag{6a}$$

$$\overleftrightarrow{S} = \overline{\overline{s}} : \overleftrightarrow{T} \tag{7a}$$

where : stands for the tensor dyadic product. GaN and AlN form in either the Wurtzite (Wz)(hexagonal) or Zincblende (cubic) crystal classes. For Wz with symmetry notations 6 mm, $C_{6v}^4, \ldots$

$$c_{ij} = \begin{bmatrix} c_{11} & c_{12} & c_{13} & 0 & 0 & 0 \\ c_{12} & c_{11} & c_{13} & 0 & 0 & 0 \\ c_{13} & c_{13} & c_{33} & 0 & 0 & 0 \\ 0 & 0 & 0 & c_{44} & 0 & 0 \\ 0 & 0 & 0 & 0 & c_{44} & 0 \\ 0 & 0 & 0 & 0 & 0 & \dfrac{c_{11} - c_{12}}{2} \end{bmatrix} \tag{8}$$

To summarize

$$\begin{bmatrix} T_1 \\ T_2 \\ T_3 \\ T_4 \\ T_5 \\ T_6 \end{bmatrix} = \begin{bmatrix} c_{11} & c_{12} & c_{13} & 0 & 0 & 0 \\ c_{12} & c_{11} & c_{13} & 0 & 0 & 0 \\ c_{13} & c_{13} & c_{33} & 0 & 0 & 0 \\ 0 & 0 & 0 & c_{44} & 0 & 0 \\ 0 & 0 & 0 & 0 & c_{44} & 0 \\ 0 & 0 & 0 & 0 & 0 & \dfrac{c_{11} - c_{12}}{2} \end{bmatrix} \begin{bmatrix} S_1 \\ S_2 \\ S_3 \\ S_4 \\ S_5 \\ S_6 \end{bmatrix} \tag{9}$$

$$\begin{bmatrix} S_1 \\ S_2 \\ S_3 \\ S_4 \\ S_5 \\ S_6 \end{bmatrix} = \begin{bmatrix} s_{11} & s_{12} & s_{13} & 0 & 0 & 0 \\ s_{12} & s_{11} & s_{13} & 0 & 0 & 0 \\ s_{13} & s_{13} & s_{33} & 0 & 0 & 0 \\ 0 & 0 & 0 & s_{44} & 0 & 0 \\ 0 & 0 & 0 & 0 & s_{44} & 0 \\ 0 & 0 & 0 & 0 & 0 & 2(s_{11} - s_{12}) \end{bmatrix} \begin{bmatrix} T_1 \\ T_2 \\ T_3 \\ T_4 \\ T_5 \\ T_6 \end{bmatrix} \tag{10}$$

The determination of the five c_{ij} values is rather difficult. Presently GaN must be grown on a substrate (Sapphire, SiC, ZnO, Si, etc.). The epitaxial growth may be MOCVD, MBE, HVPE, among others; and the growth rates, gas pressures, and temperatures vary considerably. Under the present situation the films vary greatly. They differ in stoichiometry, defects, crystal faults, surface morphology, and film thickness (nm to μm). For these reasons, among others, one may only expect ranges of values for the fundamental constants for GaN or AlN. Table I gives two sets of values for the c_{ij}. The first column was derived from acoustic velocity measurements (ref. 3) on plasma-induced MBE films on Sapphire without a nucleation layer, with thickness between 800 and 1300 nm. The second column is from best guesses after averaging entries from the literature (refs. 4 to 8).

TABLE I.—STIFFNESS CONSTANTS FOR GaN

GaN	c_{ij} in GPa	c_{ij} (average. from literature)	Difference (percent)
c_{11}	370	382	3.2
c_{12}	145	145	0
c_{13}	110	106	3.6
c_{33}	390	389	0.26
c_{44}	90	103	14
c_{66}	112.5	123	9

TABLE II.—STIFFNESS CONSTANTS FOR AlN

AlN	c_{ij} in GPa	c_{ij} (average. from literature)	Difference (percent)
c_{11}	410	390	4.9
c_{12}	140	125	10.7
c_{13}	100	120	20
c_{33}	390	395	1.28
c_{44}	120	118	1.7

Given the c_{ij} the s_{ij} are (ref. 1)

let

$$c_\Delta = c_{33}(c_{11} + c_{12}) - 2c_{13}^2 \tag{11}$$

then

$$s_{11} = \frac{1}{2}\left[\frac{c_{33}}{c_\Delta} + \frac{1}{c_{11} - c_{12}}\right] \tag{12}$$

$$s_{12} = \frac{c_{33}}{c_\Delta} - s_{11} \tag{13}$$

$$s_{13} = -\frac{c_{13}}{c_\Delta} \tag{14}$$

$$s_{33} = \frac{c_{11} + c_{12}}{c_\Delta} \tag{15}$$

$$s_{44} = \frac{1}{c_{44}} \tag{16}$$

Table III gives the s_{ij} using best guess values for the c_{ij}.

TABLE III.—COMPLIANCE COEFFICIENTS FOR GaN AND AlN.

	GaN	AlN
$s_{11}\left(\frac{m^2}{N}\times 10^{-12}\right)$	3.175	3.5319
s_{12}	−1.044	−1.0136
s_{13}	−0.58072	−0.76506
s_{33}	2.887	2.9965 (2.8 from experiment)
s_{44}	9.7087	8.474

While GaN, AlN, and $Al_x\,Ga_{1-x}\,N$ are anisotropic, many papers treat them as isotropic for simplicity. For an isotropic material, we have

$$c_{ij} = \begin{bmatrix} \lambda+2\mu & \lambda & \lambda & 0 & 0 & 0 \\ \lambda & \lambda+2\mu & \lambda & 0 & 0 & 0 \\ \lambda & \lambda & \lambda+2\mu & 0 & 0 & 0 \\ 0 & 0 & 0 & \mu & 0 & 0 \\ 0 & 0 & 0 & 0 & \mu & 0 \\ 0 & 0 & 0 & 0 & 0 & \mu \end{bmatrix} \tag{17}$$

Where λ and μ are the Lamé constants. Two other constants are normally used instead of λ and μ; namely E and ν, Young's modulus and Poisson's ratio, respectively. They are given by

$$E = \frac{\mu(3\lambda+2\mu)}{\lambda+\mu} \tag{18}$$

$$\nu = \frac{\lambda}{2(\lambda+\mu)} \tag{19}$$

The bulk modulus is defined as

$$B = \frac{3\lambda + 2\mu}{3} \tag{20}$$

The *T*/*S* relationships in terms of E and ν are (ref. 9)

$$T_{xx} = \frac{E}{(1+\nu)(1-2\nu)}\left[(1-\nu)S_{xx} + \nu\left(S_{yy} + S_{zz}\right)\right] \tag{21}$$

$$T_{yy} = \frac{E}{(1+\nu)(1-2\nu)}\left[(1-\nu)S_{yy} + \nu\left(S_{zz} + S_{xx}\right)\right] \tag{22}$$

$$T_{zz} = \frac{E}{(1+\nu)(1-2\nu)}\left[(1-\nu)S_{zz} + \nu\left(S_{xx} + S_{yy}\right)\right] \tag{23}$$

$$T_{yz} = T_{zy} = \frac{E}{(1+\nu)}S_{yz} \tag{24}$$

$$T_{zx} = T_{xz} = \frac{E}{(1+\nu)}S_{zx} \tag{25}$$

$$T_{xy} = T_{yx} = \frac{E}{(1+\nu)}S_{xy} \tag{26}$$

or

$$S_{xx} = \frac{1}{E}\left[T_{xx} - \nu\left(T_{yy} + T_{zz}\right)\right] \tag{27}$$

$$S_{yy} = \frac{1}{E}\left[T_{yy} - \nu\left(T_{xx} + T_{zz}\right)\right] \tag{28}$$

$$S_{zz} = \frac{1}{E}\left[T_{zz} - \nu\left(T_{xx} + T_{yy}\right)\right] \tag{29}$$

$$S_{yz} = \frac{(1+\nu)}{E}T_{yz} \tag{30}$$

$$S_{xy} = \frac{(1+\nu)}{E}T_{xy} \tag{31}$$

$$S_{zx} = \frac{(1+\nu)}{E}T_{zx} \tag{32}$$

There are several special cases:

Plane strain ($S_{zz} = 0$)

$$T_{xx} = \frac{E}{(1+\nu)(1-2\nu)}\left[(1-\nu)S_{xx} + \nu S_{yy}\right] \tag{33}$$

$$T_{yy} = \frac{E}{(1+\nu)(1-2\nu)}\left[(1-\nu)S_{yy} + \nu S_{xx}\right] \tag{34}$$

$$T_{zz} = \frac{E\nu}{(1+\nu)(1-2\nu)}\left[S_{xx} + S_{yy}\right] \tag{35}$$

$$T_{xy} = \frac{E}{1+\nu} S_{xy} \tag{36}$$

$$T_{yz} = T_{zy} = 0 \tag{37}$$

or

$$S_{xx} = \frac{(1+\nu)}{E}\left[(1-\nu)T_{xx} - \nu T_{yy}\right] \tag{38}$$

$$S_{yy} = \frac{(1+\nu)}{E}\left[(1-\nu)T_{yy} - \nu T_{xx}\right] \tag{39}$$

$$S_{zz} = 0 \tag{40}$$

$$S_{xy} = \frac{(1+\nu)}{E} T_{xy} \tag{41}$$

$$S_{yz} = S_{xz} = 0 \tag{42}$$

Plane stress ($T_{zz} = 0$)

$$T_{xx} = \frac{E}{1-\nu^2}\left(S_{xx} + \nu S_{yy}\right) \tag{43}$$

$$T_{yy} = \frac{E}{1-\nu^2}\left(S_{yy} + \nu S_{xx}\right) \tag{44}$$

$$T_{zz} = 0 \tag{45}$$

$$T_{xy} = \frac{E}{1+\nu} S_{xy} \tag{46}$$

$$T_{yz} = T_{xz} = 0 \tag{47}$$

or

$$S_{xx} = \frac{1}{E}\left(T_{xx} - \nu T_{yy}\right) \tag{48}$$

$$S_{yy} = \frac{1}{E}\left(T_{yy} - \nu T_{xx}\right) \tag{49}$$

$$S_{zz} = \frac{-\nu}{E}\left(T_{xx} + T_{yy}\right) \tag{50}$$

$$S_{xy} = \frac{(1+\nu)}{E} T_{xy} \tag{51}$$

$$S_{yz} = S_{xz} = 0 \tag{52}$$

We may approximate the constants λ, μ, ν, E, B, and M (the biaxial modulus) as follows. From equations (9) and (17) and table I, we see

$$c_{11} = \lambda + 2\mu = 370 = 382 \tag{53}$$

$$c_{12} = \lambda = 145 = 145 \tag{54}$$

$$c_{13} = \lambda = 110 = 106 \tag{55}$$

$$c_{33} = \lambda + 2\mu = 390 = 389 \tag{56}$$

$$c_{44} = \mu = 90 = 103 \tag{57}$$

$$c_{66} = \mu = 112.5 = 123 \tag{58}$$

From visual inspection it appears that a good choice is

$$\lambda + 2\mu \doteq 383 \tag{59}$$

and

$$\lambda \doteq 126.5 \tag{60}$$

$$\mu \doteq 128 \tag{61}$$

With this choice, and using equations (18) to (20), we find (average values denoted with a carat (^))

$$\hat{E} = 320 \tag{62}$$

$$\hat{\nu} = 0.25 \tag{63}$$

$$\hat{B} = 212 \tag{64}$$

$$\hat{M} = \frac{\mathrm{E}}{1-\nu} = 427 \tag{63a}$$

In the literature I have found the following formulas

$$B = \frac{(c_{11}+c_{12})c_{33} - 2c_{13}^2}{c_{11}+c_{12}+2c_{33}-4c_{13}} = \frac{E}{3(1-2\nu)} \tag{65}$$

$$M = \frac{E}{1-\nu} = c_{11} + c_{12} - \frac{2c_{13}^2}{c_{33}} \tag{66}$$

Note, equations (65) and (66) permit the determination of E and ν, as the c_{ij} are known, that is, two equations in the unknowns E and ν. From the values in table I, we find

Column 1 $\hat{E} = 357 \quad \hat{\nu} = 0.21 \quad \hat{B} = 206.6 \quad \hat{M} = 453$ (67)

Column 2 $\hat{E} = 377 \quad \hat{\nu} = 0.20 \quad \hat{B} = 207.2 \quad \hat{M} = 469$ (68)

From the literature I have found the following reported values.

B: 117, 160, 180, 188, 200, 204, 206, 210, 220, 268 (69)

These yield and average $\hat{B} = 195$ GPa.

ν: 0.23, 0.25, 0.38, $\hat{\nu} = 0.29$ (70)

E: 196, 290 $\hat{E} = 243$ (71)

M: 413, 450, 479, $\hat{M} = 447$ (72)

From table I of reference 10 we find

$$\begin{aligned}\hat{c}_{11} &= 363\\ \hat{c}_{12} &= 128\\ \hat{c}_{13} &= 99\\ \hat{c}_{33} &= 385\\ \hat{c}_{44} &= 85\\ \hat{B} &= 195\\ \hat{E} &= 273\\ \hat{\nu} &= 0.27\end{aligned} \tag{73}$$

and the experimental values given (ref. 10) were

$$B = 200 \pm 20$$

$$E = 290 \tag{74}$$

$$\nu = 0.23 \pm 0.06$$

TABLE IV.—ELASTIC CONSTANTS FOR AIN FROM REF. 10

	From ref. 3	Best guess	Difference (percent)
c_{11}	410	390	4.9
c_{12}	140	125	10.7
c_{13}	100	120	20
c_{33}	390	395	1.3
c_{44}	120	118	1.7

$\hat{B} = 201$

$\hat{\nu} = 0.21$

$\hat{M} = 442$

The dispersion in the basic parameters reflects the wide variation in the films due to a variety of factors, as well as attempting to forge an approximate isotropic model.

In most cases the films are assumed to be in "biaxial stress" which means

$$T_{xx} = T_{yy}, \text{and } T_{zz} = 0 \tag{75}$$

then equation (27) gives

$$S_{xx}E = T_{xx} - \nu T_{yy} = T_{xx} - \nu T_{xx}$$

$$T_{xx} = \frac{E}{1-\nu} S_{xx} \tag{76}$$

which is apparently the reason for the definition of M in equation (66). The literature often uses the notation

$$\sigma_{xx} = M_{0001} \in_{xx} \tag{77}$$

where the subscript 0001 denotes the z-direction (parallel with the c-axis of the film). The crystal is then defined as having a Ga face. From equation (9)

$$T_3 = c_{13}S_1 + c_{13}S_2 + c_{33}S_3$$

If $T_3 = 0$, a "free surface," then if $S_1 = S_2$ (biaxial strain), then

$$0 = 2c_{13}S_1 + c_{33}S_3$$

$$u_{zz} = -\frac{2c_{13}}{c_{33}}u_{xx} \tag{78}$$

This result will be used often later. It can be shown that

$$T_{xx} = \frac{2c_{13}^2 - c_{33}(c_{11} + c_2)}{2c_{13}}S_{zz} \tag{79}$$

where it is assumed that $T_{xx} = T_{yy}$, and $T_{zz} = 0$. This corresponds to equation (50)

$$T_{xx} = -\frac{E}{2\nu}S_{zz}$$

Using equations (60) and (61), $\lambda = 126.5$, $\mu = 128$, then $-E/2\nu = -639.2$. Using the values in column 2 of table I, equation (79) becomes

$$T_{xx} = -861\ S_{zz} \quad |\text{percent difference}| = 26\ \text{percent} \tag{80}$$

This demonstrates the uncertainty in the magnitudes of the quantities in this section.

Estimation of Stress and Strain

We assume the stress in the layers may be conceptually described by the superposition of three components:

$$\sigma_{TOTAL} = \sigma_{EXTERNAL} + \sigma_{THERMAL} + \sigma_{INTRINSIC} \tag{81}$$

The thermal part is the most straightforward, it is

$$\sigma_{THERMAL} = \sigma_{TH} = \Delta\alpha\Delta T\frac{E}{1-\nu} \tag{82}$$

Where $\Delta\alpha$ is the difference in thermal expansion coefficients (TEC), between the layers. Also ΔT is the difference between the growth temperature and the sample temperature (generally room temperature (RT)). The above assumes the substrate and epilayer are relaxed at the growth temperature (not true in general), and that no relaxation during cooling has taken place.

The external portion (σ_{EXT}) is due to loading by adjacent layers; lattice mismatch, metal pads, and any recognizable force. The last term is referred to as intrinsic or residual stress; it acts as a catch-all for stresses that do not fit into the two previous categories. The residual stresses are difficult to handle because they depend on growth parameters, which differ greatly for the basic growth methods. The basic methods are MBE, MOCVD, HVPE, and variations of them. Some of the parameters are growth temperature, pressure, gas flow rates, substrate crystal orientation, surface conditions, and preparation procedure. The GaN is often grown on a nucleation layer of either GaN or AlN. The properties of the nucleation layer include thickness, growth temperature, and doping. Finally, defects produced by vacancies, cracks, misfit dislocations, threading dislocations, etc.

After the stress has been quantified the strain will still not be known exactly, as the material responds to stress in at least two ways. One is to strain via Hooke's law, the other is to generate defects and propagate them throughout the material (relaxation). Finally, cracks do occur in GaN and sapphire, and many in the GaN are not visible by observation of the surface.

External Stress/Strain

Most often the strain due to lattice mismatch is assumed to be the dominant factor. Define the misfit parameter

$$f_m = \frac{a - a_0}{a_0} \tag{83}$$

where a_0 is the relaxed lattice parameter and a is the strained value. The strain is then

$$\epsilon_{xx} = \pm f_m \tag{84}$$

where the appropriate sign is chosen. Maeda (ref. 11) introduced a "lattice relaxation ratio, R" by

$$\epsilon_{xx} = \frac{\Delta a}{a_0}(1 - R) \tag{85}$$

This is very useful, as it permits some relaxation at the interfaces. The corresponding stresses are

$$\sigma_{xx} = -\frac{E}{2\nu}\frac{\Delta c}{c_0} = -\frac{E}{2\nu}\epsilon_{zz} \tag{86}$$

$$\sigma_{xx} = -\frac{E}{1-\nu}\frac{\Delta a}{a_0} = M\,\epsilon_{xx} \tag{87}$$

where $\Delta c/c_0$ is the strain along the c-axis, and $\Delta a/a_0$ is that in the basal plane. The composite stress in a given film, or layers of film may be calculated at several levels of approximation. We start with Etzkorn (ref. 12).

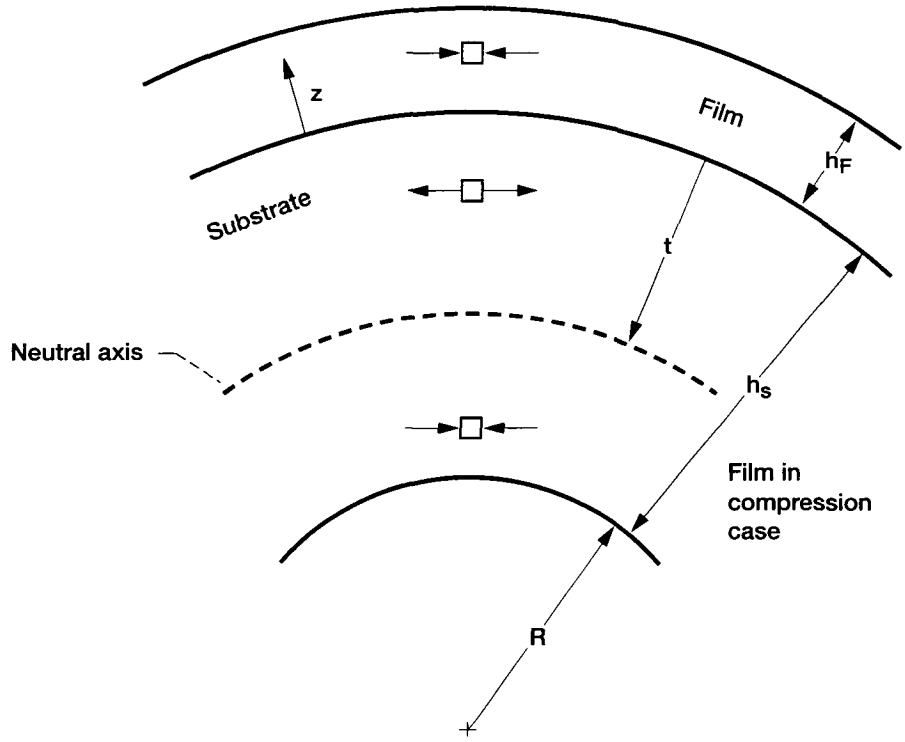

Figure 1.—Epitaxial film of thickness h_F on a substrate of thickness h_S. Coordinate axes in the layers are z and t, respectively. Bending is due to differing thermal expansion coefficients.

The figure is for the case when the net stress is compressive. The subscripts F an S represent film and substrate, respectively. The equations are as follows.

Define the parameter

$$r = \frac{[E_F/(1-\nu_F)]h_F}{[E_S/(1-\nu_S)]h_S} = \frac{M_F h_F}{M_S h_S} \tag{88}$$

Assume the thermal strain dominates

$$\sigma_F = -M_F \frac{\Delta\alpha\Delta T}{1+r} \tag{89}$$

$$\sigma_S = M_S \frac{\Delta\alpha\Delta T}{1+r} r \tag{90}$$

$$\epsilon_S^{RT} = \frac{(\alpha_F - \alpha_S)\Delta T}{1+r} \tag{91}$$

$$\epsilon_S^{RT} = \frac{(\alpha_F - \alpha_S)\Delta T}{1+r} r \tag{92}$$

$$t = \frac{h_S - h_F r}{2(1+r)} \tag{93}$$

$$R = \frac{1}{\Delta\alpha\Delta T}\left[\frac{h_S^2}{6(h_S - 2t)} + \frac{h_F^2}{6(h_F + 2t)} + \frac{1}{2}(h_S + h_F)\right] \tag{94}$$

$$\epsilon_F(z) = \epsilon_F^{RT} + \frac{z + t}{R} \tag{95}$$

Notice equation (95) gives the strain as a linear function of distance z from the interface. Equation (94) gives the radius of curvature. Observe that this formulation only requires material parameters and the thickness of the substrate and film.

Next, the equation of Skromme (ref. 13):

$$\sigma_{\text{SURFACE}} = -\frac{M_S h_S^3 + M_F h_F^3 - 3M_F h_F^2 (h_S + h_F)}{6(h_S + h_F) h_F R} \tag{96}$$

where R is the radius of curvature which must be measured. Kozawa (ref. 14) has a slightly simpler form (assumes ν the same in both layers)

$$\sigma_F = \frac{E_S h_S^3 + E_F h_F^3}{6(1 - \nu)(h_S + h_F) h_F R} \tag{97}$$

TABLE V.—DATA FROM REF. 14 WITH OTHER ENTRIES IN PARENTHESES

	Sapphire	GaN
h_F, h_S (μ)	300	2.5 to 48.8
E (GPa)	425	196 (295)
TEC (10^{-6})	7.5	5.45
ν	0.3 (0.25)	0.3 (0.25)

From Hearne (ref. 15) we have Stoney's formula:

$$\sigma_F = \frac{M_S h_S^2}{6 h_F R} \tag{98}$$

where for MOCVD at 1050 °C; sapphire: M = 450 or 479, depending on wafer; 6H-SiC: M = 586 GPa. Then

$$\sigma_F = \sigma_{xx} = M_F \epsilon_{xx} \tag{99}$$

The composite stress was measured to be tensile with range

$$0.14 < \sigma_{xx} < 0.29 \text{ GPa}$$

The thermal component (by measurements) was -0.66 ± 1 GPa, and the theoretical thermal component is -1.4 ± 0.7 GPa. Thus, the residual and perhaps some lattice portion dominates the stress in the given films. The radius of curvature R is determined by surface profilometry or laser reflection. Generally

$$2 \text{ m} < R < 20 \text{ m}$$

and in most cases $R < 6$ m. However, $R = 0.58$ m for HVPE films.

Some experimental data (though incomplete) is helpful. From reference 16 a sample consisting of a 6H-SiC substrate with 3μ of porous GaN, then 3μ of HVPE GaN on top. The surface was in tension (wafer like a cup that holds water). The radius of curvature R was -6.5 m, the in-plane stress was 0.64 GPa, and the strain along the c-axis was -1.12×10^{-3}. The substrate thickness was not given.

A common range of parameters for GaN on sapphire is: 250 μm of sapphire with 500 Å of AlN nucleation layer, and 1 to 5 μm of GaN. The residual strain in the GaN is of the order of 1.0×10^{-4}.

General Case of Several Layers

For the general case of several layers, one may use the results of Olsen and Ettenberg (ref. 17). The stress in any layer may be estimated from (see fig. 2)

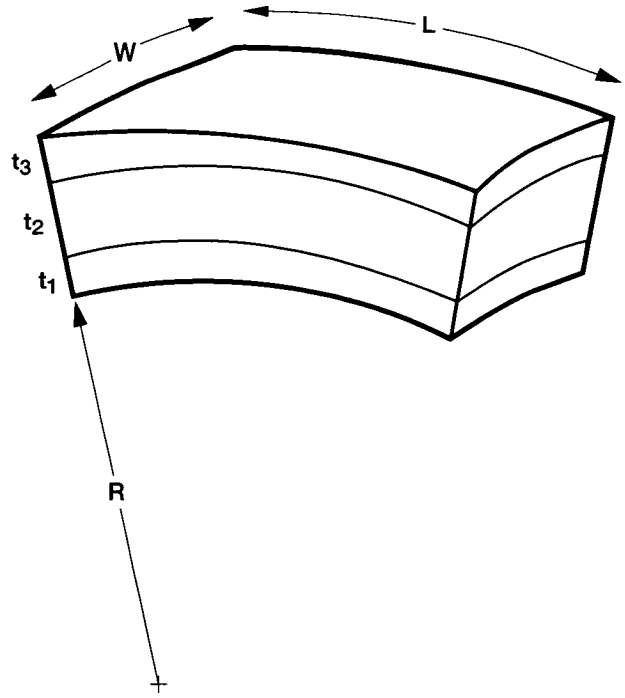

Figure 2.—General layer structure with thickness t_j for each layer. Measured radius of curvature is R.

$$\sigma_j(y) = E\left[\sum_{i=1}^{N}\left(\frac{t_i \in_{ij}}{t} + \frac{t_i \kappa_i}{2R}\right) + \frac{y - \frac{t_j}{2}}{2R}\right] \tag{100}$$

Here it is assumed that the elastic moduli (Young's moduli) of all layers are the same and equal to E. In equation (100) y is measured from the bottom of the j^{th} layer. The terms in equation (100) are

$$t = \sum_{i=1}^{N} t_i \tag{101}$$

$$R = t^3 \left(6 \sum_{i=1}^{N} \sum_{j>1}^{N} t_i t_j \in_{ij} \right)^{-1} \tag{102}$$

$$\begin{aligned} \kappa_i &= 1 \quad i < j \\ \kappa_i &= 0 \quad i = j \\ \kappa_i &= -1 \quad i > j \end{aligned} \tag{103}$$

In equation (102) the strain at the interface of the i^{th} and j^{th} layer $\in_{ij}$ is related to the measured radius of curvature. However, it is assumed the strains $\in_{ij}$ are known, along with the thickness t_i of each layer. If $w \sim L$, then one may assume spherical bending, then a two-dimensional (2D) solution may be obtained from the given one-dimensional (1D) by

$$\sigma_i(y)_{2D} = \frac{\sigma_j(y)_{1D}}{1 - \nu} \tag{104}$$

Reasonable choices for the interface strains are the larger of thermal, lattice mismatch, or residual strains (ref. 18). The reviews in references 19 to 22 should be consulted for more information.

2. Piezoelectricity

This section details equations we will use later. It is important to note that this discussion treats dielectrics, not semiconductors, that is, effects of carrier screening are ignored. We start with the defining equation for $\overline{D}, \overline{E}$, and $\overline{P}$.

$$\overline{D} = \in_0 \overline{E} + \overline{P} \tag{105}$$

Here

$$\overline{P} = \overline{P}_{\text{ELECTRONIC}} + \overline{P}_{\text{IONIC}} + \overline{P}_{\text{OTHER}} \tag{106}$$

In most cases only the first two terms in equation (106) are assumed to exist, and $\overline{P}_{\text{OTHER}}$ is assumed equal to zero. This case then has the constitutive assumption that the polarization is linearly related to the $\overline{E}$ field,

$$\overline{P}_{\text{ELECTRONIC}} + \overline{P}_{\text{IONIC}} \underline{\underline{\Delta}} \in_0 \chi_e \overline{E} \tag{107}$$

where χ_e is the polarizability. Then

$$\begin{aligned}\overline{D} &= \epsilon_0 \overline{E} + \epsilon_0 \chi_e \overline{E} \\ &= \epsilon_0 \epsilon_r \overline{E} \quad \left(\overline{P}_{\text{OTHER}} \triangleq 0\right)\end{aligned} \tag{108}$$

which is the normal case. For anisotropic material we write

$$\frac{1}{\epsilon_0}\begin{bmatrix} D_x \\ D_y \\ D_z \end{bmatrix} = \begin{bmatrix} \kappa_{xx} & \kappa_{xy} & \kappa_{xz} \\ \kappa_{yx} & \kappa_{yy} & \kappa_{yz} \\ \kappa_{zx} & \kappa_{zy} & \kappa_{zz} \end{bmatrix}\begin{bmatrix} E_x \\ E_y \\ E_z \end{bmatrix} \tag{109}$$

We use κ since ϵ is used so often for strain. Thus

$$\frac{1}{\epsilon_0}\overline{D} = \overleftrightarrow{\kappa} \cdot \overline{E} \tag{110}$$

or

$$\frac{1}{\epsilon_0} D_j = \kappa_{ij} E_j \qquad i, j = x, y, z$$

for GaN and AlN, we have (ref. 20)

$$\begin{bmatrix} \kappa_{11} & 0 & 0 \\ 0 & \kappa_{11} & 0 \\ 0 & 0 & \kappa_{33} \end{bmatrix} \tag{111}$$

for GaN, $\kappa_{11} = 9.5$ and $\kappa_{33} = 10.4$
for AlN, $\kappa_{11} = 9.0$ and $\kappa_{33} = 10.7$

Now when the dielectric material is also piezoelectric (following Auld, (ref. 1))

$$\begin{aligned}\overleftrightarrow{S} &= d_T \cdot \overline{E} + s^E : \overleftrightarrow{T} \\ \overline{D} &= \epsilon_0 \kappa^T \cdot \overline{E} + d : \overleftrightarrow{T}\end{aligned} \tag{112}$$

which are the piezoelectric strain equations. Another form is

$$\begin{aligned}\overleftrightarrow{T} &= -e : \overline{E} + c^E : \overleftrightarrow{S} \\ \overline{D} &= \epsilon_0 \kappa^S \cdot \overline{E} + e : \overleftrightarrow{S}\end{aligned} \tag{113}$$

which are the corresponding stress equations. The superscripts mean constant electric field $\overline{E}$, constant stress $\overleftrightarrow{T}$, or constant strain $\overleftrightarrow{S}$. By inspection we observe (now $\overline{P}_{\text{OTHER}} = \overline{P}_{\text{PIEZOELECTRIC}}$)

$$\overline{P} = d : \overleftrightarrow{T} \tag{114}$$

where d_{ij} are the piezoelectric strain constants. We also have

$$\overline{P} = e : \ddot{S} \tag{115}$$

where e_{ij} are the stress constants. For our Wz crystals we have (refs. 1 and 23)

$$\begin{bmatrix} P_x \\ P_y \\ P_z \end{bmatrix} = \begin{bmatrix} 0 & 0 & 0 & 0 & d_{15} & 0 \\ 0 & 0 & 0 & d_{15} & 0 & 0 \\ d_{31} & d_{31} & d_{33} & 0 & 0 & 0 \end{bmatrix} \begin{bmatrix} T_1 \\ T_2 \\ T_3 \\ T_4 \\ T_5 \\ T_6 \end{bmatrix} \tag{116}$$

with the associations $T_1 = \sigma_1 = \sigma_{xx}$, $T_2 = \sigma_2 = \sigma_{yy}$, $T_3 = \sigma_3 = \sigma_{zz}$, $T_4 = \sigma_4 = \sigma_{yz}$, $T_5 = \sigma_5 = \sigma_{xz}$, $T_6 = \sigma_6 = \sigma_{xy}$
As in section 1, the range of the coefficients is large.

The following strain constants are in units of 10^{-10} cm/V (see refs. 22 to 26):

TABLE VI.—PIEZOELECTRIC STRAIN CONSTANTS OF GaN

	Measured	Calculated	Estimated	Bulk	Clamped	Polycrystal
d_{31}	−0.9	−1.16	−1.7	−1.9	−1.4	−1.0
d_{33}		2.39		3.7	2.8	2.0
d_{15}	−3.1	−2.75				

The following strain constants are in units of 10^{-10} cm/V:

TABLE VII.—PIEZOELECTRIC STRAIN CONSTANTS OF AlN

	Measured	Calculated	Estimated	Bulk	Clamped	Polycrystal
d_{31}	−2.0	−2.65	−2.71	−2.8	−2.0	−2.71
d_{33}	5.0	5.53	6.72	5.6	4.0 (3.2 film)	
d_{15}		−3.4				−3.6

Theory says $d_{31} = -(1/2)\, d_{33}$. The alternate representation is

$$\overline{P} = e : \ddot{S}$$

or

$$\begin{bmatrix} P_x \\ P_y \\ P_z \end{bmatrix} = \begin{bmatrix} 0 & 0 & 0 & 0 & e_{15} & 0 \\ 0 & 0 & 0 & e_{15} & 0 & 0 \\ e_{31} & e_{31} & e_{33} & 0 & 0 & 0 \end{bmatrix} \begin{bmatrix} u_{xx} \\ u_{yy} \\ u_{zz} \\ u_{yz} \\ u_{zx} \\ u_{xy} \end{bmatrix} \tag{117}$$

The following stress constants are in units of C/m^2:

TABLE VIII.—PIEZOELECTRIC STRESS CONSTANTS OF GaN

	Literature	Bulk	Crystal	Clamped	Polycrystal
e_{15}	−0.21 −0.3 −0.33				
e_{31}	−0.22 −0.33 −0.36 −0.49	−0.55	−0.41		−0.3
e_{33}	0.44 0.65 0.73 1.0	1.12		0.85	0.6

The following stress constants are in units of C/m^2:

TABLE IX.—PIEZOELECTRIC STRESS CONSTANTS OF AlN

	Literature	Bulk	Crystal	Clamped	Polycrystal
e_{31}		−0.6		−0.63	−0.5
e_{33}	1.46	1.5		1.06 0.85	

Also

$$d_T \cdot \overline{E} = \begin{bmatrix} 0 & 0 & d_{31} \\ 0 & 0 & d_{31} \\ 0 & 0 & d_{33} \\ 0 & d_{15} & 0 \\ d_{15} & 0 & 0 \\ 0 & 0 & 0 \end{bmatrix} \begin{bmatrix} E_x \\ E_y \\ E_z \end{bmatrix} \tag{118}$$

It can be shown that

$$e_{Jj} = c_{JI} d_{Ij} \tag{119}$$

Using this relationship we may determine the d_{ij}

$$
\begin{aligned}
d_{31} &= e_{31}s_{11} + e_{32}s_{21} + e_{33}s_{31} + \overset{\uparrow}{e}_{34}^{0}\, s_{41} + \overset{\uparrow}{e}_{35}^{0}\, s_{51} + \overset{\uparrow}{e}_{36}^{0}\, s_{61} \\
&= e_{31}(s_{11} + s_{21}) + e_{33}s_{31} = (-0.35)\left(2.131\times10^{-12}\right) + (0.705)\left(-5.8072\times10^{-12}\right) \\
&= -1.16\times10^{-10}\ \text{cm/V} = -1.16\times10^{-12}\ \text{C/N} \\
d_{33} &= e_{31}s_{13} + e_{32}s_{23} + e_{33}s_{33} + \overset{\uparrow}{e}_{34}^{0}\, s_{43} + \overset{\uparrow}{e}_{35}^{0}\, s_{53} + \overset{\uparrow}{e}_{36}^{0}\, s_{63} \\
&= 2e_{31}s_{13} + e_{33}s_{33} = 2.39\times10^{-12}\ \text{C/N} \\
d_{15} &= \overset{\uparrow}{e}_{11}^{0}\, s_{15} + \overset{\uparrow}{e}_{12}^{0}\, s_{25} + \overset{\uparrow}{e}_{13}^{0}\, s_{35} + \overset{\uparrow}{e}_{14}^{0}\, s_{45} + \overset{\uparrow}{e}_{15}^{0}\, s_{55} + \overset{\uparrow}{e}_{16}^{0}\, s_{65} \\
&= e_{15}s_{44} = -2.75\times10^{-12}\ \text{C/N}
\end{aligned}
$$

In our application, one often assumes the GaN to be completely relaxed, and the AlGaN to be in tensile biaxial strain. The resulting polarization field at the AlGaN/GaN interface is assumed to be as shown below. Start with

$$P_z = e_{31}u_{xx} + e_{31}u_{yy} + e_{33}u_{zz} \tag{120}$$

Next assume a free surface (this implies the top of the AlGaN layer is free). This is a questionable assumption as the gate metallization loads the layer. Next assume biaxial strain, $u_{xx} = u_{yy}$

$$\therefore u_{zz} = -2\frac{c_{13}}{c_{33}}u_{xx} \tag{121}$$

which is equation (78) of section 1. Then

$$P_z = 2e_{31}u_{xx} - 2\frac{c_{13}}{c_{31}}u_{xx}e_{33} = 2\left[e_{31} - e_{33}\frac{c_{13}}{c_{33}}\right]u_{xx} \tag{122}$$

The term in brackets has been measured to be –0.3 C/m^2. An alternate representation starts with

$$P_z = d_{31}\sigma_{xx} + d_{31}\sigma_{yy} + d_{33}\sigma_{zz} \tag{123}$$

but

$$\sigma_{xx} = c_{11}u_{xx} + c_{12}u_{yy} + c_{13}u_{zz} \tag{124}$$

and assume biaxial stress conditions hold $\sigma_{xx} = \sigma_{yy}$. Then

$$P_z = 2d_{31}(c_{11} + c_{12})u_{xx} + d_{31}c_{13}u_{zz} + d_{33}\sigma_{zz} \tag{125}$$

Next assume a free surface, so $\sigma_{zz} = 0$,

$$u_{zz} = -2\frac{c_{13}}{c_{33}}u_{xx} \tag{126}$$

then

$$P_z = 2d_{31}(c_{11} + c_{12})u_{xx} + c_{13}\left(-2\frac{c_{13}}{c_{33}}\right)u_{xx}d_{31} \tag{127}$$

finally

$$P_z = 2d_{31}\left[c_{11} + c_{12} - \frac{c_{13}^2}{c_{33}}\right]u_{xx} \tag{128}$$

The corresponding electric field is (assuming $\overline{D} = 0$, which means no charge is present)

$$E_z = -\frac{P_z}{\in_0 \in_r} = -\frac{2d_{31}}{\in_0 \in_r}\left[c_{11} + c_{12} - \frac{c_{13}^2}{c_{33}}\right]u_{xx} \tag{129}$$

This field is about 6×10^6 V/cm. equations 128 and 129 are found in the literature, (refs. 5, 27, and 28), and many have a factor of two before the c_{13}^2/c_{33} term. I interpret them as errors by attempting to add u_{xx} and u_{yy} together as the "net strain" in the basal plane. For our case of $Al_x\ Ga_{1-x}N$, some authors multiply the P_z in equation (128) by the mole fraction x to obtain the effective value.

With the preceding concepts in place, we may introduce the entire set of equations to be solved in the GaN/AlGaN system. The first group consists of the mechanical equations of equilibrium (ref. 29)

$$\begin{aligned}
\frac{\partial \sigma_{xx}}{\partial x} + \frac{\partial T_{yx}}{\partial y} + \frac{\partial T_{zx}}{\partial z} - qn\frac{\partial \phi}{\partial x} = 0 \\
\frac{\partial T_{xy}}{\partial x} + \frac{\partial \sigma_{yy}}{\partial y} + \frac{\partial T_{zy}}{\partial z} - qn\frac{\partial \phi}{\partial y} = 0 \\
\frac{\partial T_{xz}}{\partial x} + \frac{\partial T_{yx}}{\partial y} + \frac{\partial \sigma_{zz}}{\partial z} - qn\frac{\partial \phi}{\partial z} = 0
\end{aligned} \tag{130}$$

The last term in each equation is the "body force," which we assume is the charge density times the electric field. Next, the electromechanical constitutive equations are

$$\begin{bmatrix} \sigma_{xx} \\ \sigma_{yy} \\ \sigma_{zz} \\ T_{yz} \\ T_{zx} \\ T_{xy} \end{bmatrix} = \begin{bmatrix} C_{11} & C_{12} & C_{13} & 0 & 0 & 0 \\ C_{12} & C_{11} & C_{13} & 0 & 0 & 0 \\ C_{13} & C_{13} & C_{33} & 0 & 0 & 0 \\ 0 & 0 & 0 & C_{44} & 0 & 0 \\ 0 & 0 & 0 & 0 & C_{44} & 0 \\ 0 & 0 & 0 & 0 & 0 & \frac{C_{11}-C_{12}}{2} \end{bmatrix} \begin{bmatrix} \in_{xx} \\ \in_{yy} \\ \in_{zz} \\ \gamma_{yz} \\ \gamma_{zx} \\ \gamma_{xy} \end{bmatrix} - \begin{bmatrix} 0 & 0 & e_{31} \\ 0 & 0 & e_{31} \\ 0 & 0 & e_{33} \\ 0 & e_{15} & 0 \\ e_{15} & 0 & 0 \\ 0 & 0 & 0 \end{bmatrix} \begin{bmatrix} E_x \\ E_y \\ E_z \end{bmatrix} \tag{131}$$

$$\begin{bmatrix} D_x \\ D_y \\ D_z \end{bmatrix} = \epsilon_0 \begin{bmatrix} \kappa_{11} & 0 & 0 \\ 0 & \kappa_{11} & 0 \\ 0 & 0 & \kappa_{33} \end{bmatrix} \begin{bmatrix} E_x \\ E_y \\ E_z \end{bmatrix} + \begin{bmatrix} 0 & 0 & 0 & 0 & 0 & 0 \\ 0 & 0 & 0 & e_{15} & 0 & 0 \\ e_{31} & e_{31} & e_{33} & 0 & 0 & 0 \end{bmatrix} \begin{bmatrix} \epsilon_{xx} \\ \epsilon_{yy} \\ \epsilon_{zz} \\ \gamma_{yz} \\ \gamma_{zx} \\ \gamma_{xy} \end{bmatrix} \tag{132}$$

$$\begin{aligned} &\frac{\partial u}{\partial x} = \epsilon_{xx}, \frac{\partial v}{\partial y} = \epsilon_{yy}, \frac{\partial w}{\partial z} = \epsilon_{zz} \\ &\frac{\partial v}{\partial z} + \frac{\partial w}{\partial y} = \gamma_{yz}, \frac{\partial u}{\partial z} + \frac{\partial w}{\partial x} = \gamma_{zx}, \frac{\partial u}{\partial y} + \frac{\partial v}{\partial x} = \gamma_{xy} \end{aligned} \tag{133}$$

which couple the stress, strain, electric field, and electric displacement. The latter expressions are the compatibility expressions (ref. 29) relating strains to the material displacements. Notice the notation for mechanical displacements uses u, v and w; rather than just u with a subscript. The last expressions to be used are the continuity, Gauss, and current equations.

$$\begin{aligned} E_x &= -\frac{\partial \phi}{\partial x} & \frac{\partial J_x}{\partial x} + \frac{\partial J_y}{\partial y} + \frac{\partial J_z}{\partial z} &= 0 \\ E_y &= -\frac{\partial \phi}{\partial y} & J_x &= \mu_x n(\bar{r}) E_x + D_n \frac{\partial n(\bar{r})}{\partial x} \\ E_z &= -\frac{\partial \phi}{\partial z} & J_y &= \mu_y n(\bar{r}) E_y + D_n \frac{\partial n(\bar{r})}{\partial y} \\ & & J_z &= \mu_z n(\bar{r}) E_z + D_n \frac{\partial n(\bar{r})}{\partial z} \end{aligned} \tag{134}$$

$$\frac{\partial D_x}{\partial x} + \frac{\partial D_y}{\partial y} + \frac{\partial D_z}{\partial z} = qn(\bar{r}) \tag{135}$$

$$n = n(\bar{r}) = n(x, y, z) \frac{e^-}{\text{cm}^3} \tag{136}$$

where we have assumed just electrons are present. Similar terms for holes may be added for the most general case. Notice, we have 20 equations in 20 unknowns. This is an extension of the general elasticity problem to include a piezoelectric semiconductor. In elasticity theory, one has 15 equations in 15 unknowns.

The total set of equations has been provided for the sake of completeness. In principle they would be solved along with Poisson's and Schrodinger's equations in the Poisson-Schrodinger solver which presently exists in the software package.

3. Spontaneous Polarization

There is some uncertainty about spontaneous polarization, $\overline{P}_{\mathrm{SPON}}$, (see refs. 30 to 41). Bernardini et al., have performed ab initio calculations for spontaneous polarization in nitrides (refs. 30 to 34). Reference 34 discusses some of the controversial issues on the subject. On page 912 of (ref. 37) we quote "The latter distortion—henceforth called internal strain—determines a preferred polarity of the tetragonal axis and is responsible for the occurrence of spontaneous polarization." I interpret the discussion to mean that there is an alteration of the position of atoms in a cell, which is deemed an internal strain (not apparent macroscopically), which causes the spontaneous polarization. From reference 38, "The so-called pyroelectric fields then arise from the temperature dependence of the spontaneous polarization when the temperature is changed." Figure 1 in reference 39 shows both a macroscopic strain $\in$ and an internal strain u. Apparently u may exist when $\in = 0$, so a polarization may exist due solely to u; which would be a (macroscopically) strain-free polarization (spontaneous). A procedure to measure $\overline{P}_{\mathrm{SPON}}$ is given in reference 41.

$\overline{P}_{\mathrm{SPON}}$ is screened by charges adsorbed onto the surfaces of the material, as well as being screened by free charge in the bulk. It is assumed (or defined) to be either uniform or zero in the bulk. One paper, not referenced here, stated it was zero in the bulk. Its presence is known only at interfaces with other materials (air being one of them). Pyroelectricity is the production of an electric field between two surfaces of the material held at different temperatures.

$$\overline{P}_{\mathrm{PYRO}} = \overline{p}\,\Delta\,\mathrm{Temperature} \tag{137}$$

$$= \left(p_x \overline{a}_x + p_y \overline{a}_y + p_z \overline{a}_z\right)\Delta T \tag{138}$$

For GaN

$$p_x = p_y = 10^4 \frac{V}{m \cdot K} \qquad \text{basal plane}$$

$$p_z = 7 \times 10^5 \frac{V}{m \cdot K} \qquad \text{along the c-axis}$$

Both Wz $Al_xGa_{1-x}N$ and GaN possess $\overline{P}_{\mathrm{SPON}}$, and at their interface a positive bound surface charge exists (cubic GaN is piezoelectric but does not possess spontaneous polarization). This assumes a Ga face (only case we consider). This immobile charge is assumed (calculated) to reside in a layer 3 to 4 Å thick, (I will draw it in the $Al_xGa_{1-x}N$ region for clarity). Figure 3 depicts two ideal samples with their bound polarization charges (no screening).

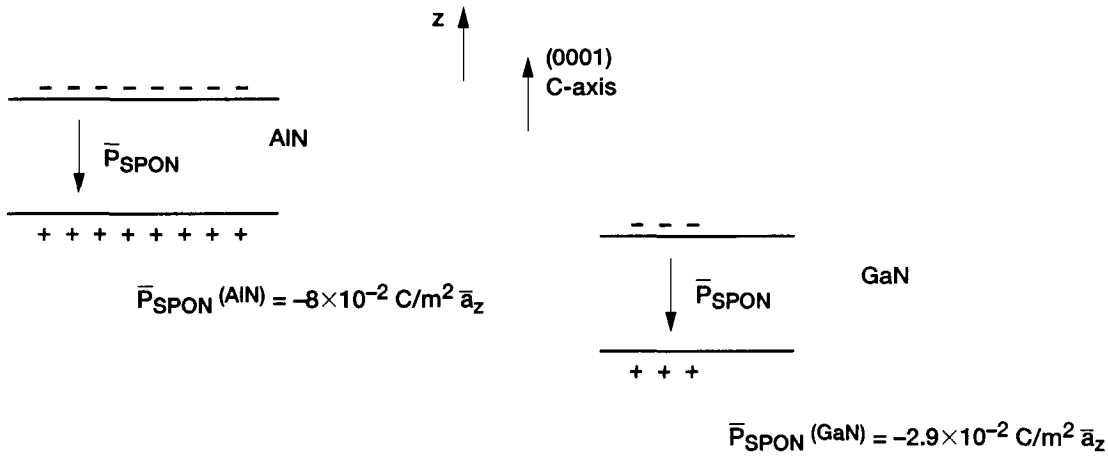

Figure 3.—Ideal samples of AlN and GaN illustrating spontaneous polarizations.

Note the z-axis and the c-axis are collinear. This relationship was assumed by Bernardini et al., and is important with respect to algebraic signs. Recall that the polarization vector $\bar{P}$ is defined to originate on negative bound charge and terminate on positive bound charge. The materials are assumed to grow from the bottom and increase in thickness as one moves up the c-axis (0001). From a simple charge superposition argument, a net positive bound charge density $\sigma(SURF)$ exists at the surface. Analytically, we have

$$\begin{aligned}\sigma_{SURF} &= (8-2.9)\times10^{-2}\ \text{C/m}^2 = 5.1\times10^{-2}\ \text{C/m}^2 \\ &= 3.19\times10^{13}\ e/\text{cm}^2\end{aligned} \tag{139}$$

Recall that at a boundary (see fig. 4)

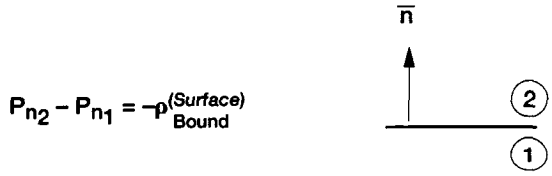

Figure 4.—Definition for bound surface charge at interface between two polarized dielectrics. Here $\bar{P}_2 \cdot \bar{n} = P_{n_2}$, . . .

For our case

$$\begin{aligned}&P_{n_2} = \bar{P}_2 \cdot \bar{n} = \left(-8\times10^{-2}\,\bar{a}_z\right)\cdot\bar{a}_z = -8\times10^{-2}\ \text{C/m}^2 \\ &P_{n_1} = \bar{P}_1 \cdot \bar{n} = \left(-2.9\times10^{-2}\,\bar{a}_z\right)\cdot\bar{a}_z = -2.9\times10^{-2}\ \text{C/m}^2 \\ &\therefore P_{n_2} - P_{n_1} = -8\times10^{-2} + 2.9\times10^{-2} = -5.1\times10^{-2}\ \text{C/m}^2 \\ &\therefore -5.1\times10^{-2}\ \text{C/m}^2 = -\rho^{(\text{SURFACE})}_{\text{BOUND}} \\ &\therefore \rho^{(\text{SURFACE})}_{\text{BOUND}} \triangleq \sigma(\text{SURF}) = 5.1\times10^{-2}\ \text{C/m}^2\end{aligned} \tag{140}$$

Figure 5 summarizes the situation.

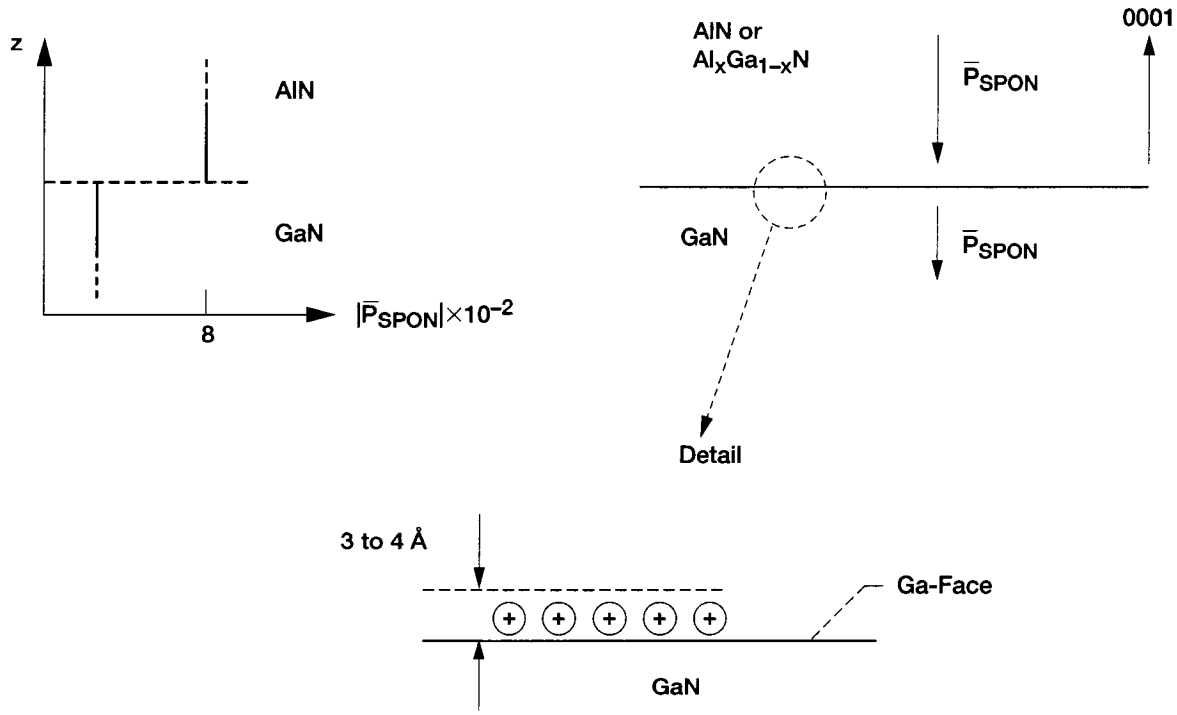

Figure 5.—Ideal situation at AlN-GaN interface. Positive surface of AlN is reduced by negative charge on GaN surface. Result is a net positive charge at interface.

Notice that the bound surface charge density is of the order of magnitude of the surface density of electrons in HEMT structures.

Several papers, and in particular reference 40, have stated that the ab initio values should be reduced by at least a factor of 2. One reason put forth is that there may exist inversion domains at the interface, as well as islands of zincblende (cubic), observed experimentally, dispersed throughout the Wz phases. Other causes can of course be put forth; impurities and surface defects. It is also assumed (stated in one paper) that

$$\nabla \cdot \bar{P}_{SPON} = 0 \tag{141}$$

as no bound volume charge density exists. This assumption seems reasonable if the internal strain is uniform and hence has no divergence. However, note that this assumption may be subject to future criticism.

4. Poisson-Schrodinger Solver

Figure 6 gives the coarse, initial band diagram in the region near the heterojunction. A key parameter is the step height ΔE_C at the interface. Anderson's model is presently used in some software, which gives the step the value

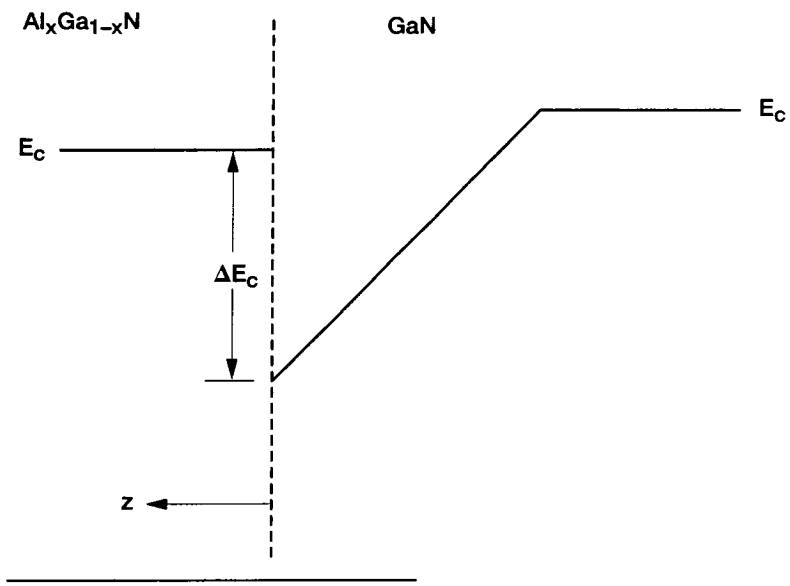

Figure 6.—Ideal triangular well for confinement of 2DEG at interface of $Al_xGa_{1-x}N$ and GaN layers. Conduction band edges are denoted as E_C.

$$\Delta E_C = \left| \chi_{Al_xGa_{1-x}N} - \chi_{GaN} \right| \tag{142}$$

where χ is the electron affinity. We will discuss alternative ways to estimate ΔE_C in later sections. The triangular well is composed of the step and the sloping side. The linear variation means a constant electric field is present. Apparently the establishment of the field comes about as follows. At the heterojunction, the step in E_C along with the position of the Fermi level causes electrons to accumulate in the notch. The region into the bulk on the left is therefore depleted, and the existing donors establish the field. The field is modeled by the standard depletion approximation

$$E(0) = \frac{q}{\epsilon}\left[N_D = \eta N_S\right] \tag{143}$$

where

N_D = depletion region sheet density
N_S = free carrier sheet density
η = a weighting factor (~0.5 to 0.8)

GaAs value at the heterojunction is

$$E(0) = 2.39 \times 10^6 \text{ V/m} \tag{144}$$

For our case of $Al_xGa_{1-x}N/GaN$, the situation is apparently quite different. From Sacconi (ref. 42), if we initially neglect all polarization, then the step height and Fermi levels (for typical doping) are not sufficient for a notch to form. Then electrons do not accumulate and create the 2DEG. After adding the spontaneous and piezoelectric factors, the notch forms, and the 2DEG is present. Apparently a depletion region does not form, as the polarization charge is sufficient to establish the field. If one does form, perhaps it is swamped by the polarization charge. One may look at the situation as follows: the 2DEG

forms to screen the bound spontaneous and piezoelectric charge residing at the interface. This introduces the question, "where do the electrons come from that establish the 2DEG?" There are valid reasons that state they cannot come from the bulk GaN, so apparently they come from donors somewhere in the $Al_xGa_{1-x}N$ region. This is not a trivial issue, as charge neutrality must hold, but the bookkeeping is not generally agreed upon in the literature. Instead of using the field expression developed from the depletion approximation, authors assume it should be represented by equation (129) in section 2,

$$E_z = -\frac{2d_{31}}{\epsilon_0 \epsilon_r}\left[c_{11} + c_{12} - \frac{c_{13}^2}{c_{33}}\right]u_{xx} \tag{145}$$

If the strain in the $Al_xGa_{1-x}N$ is tensile $u_{xx} > 0$, then the field is oriented toward the bulk just as in the case of the depletion approximation. Figure 7 summarizes the discussion.

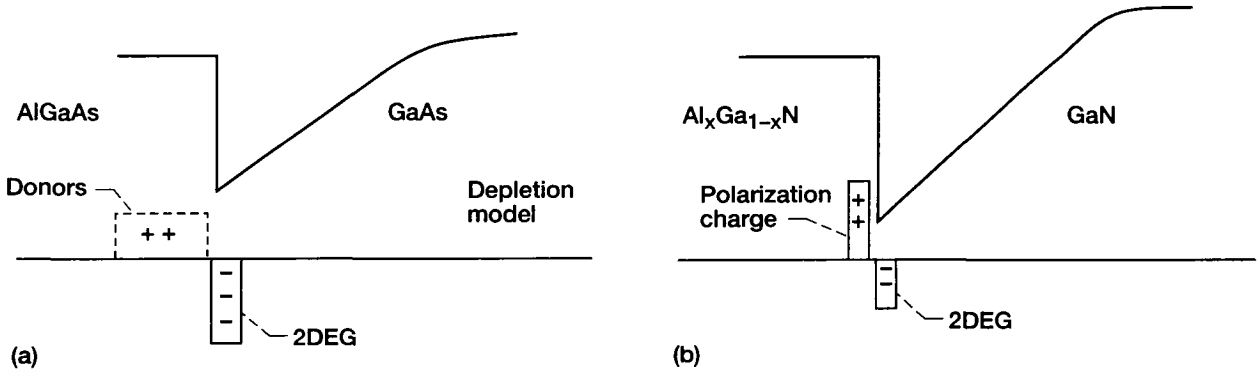

Figure 7.—2DEG formation. (a) By intentional doping. (b) By polarization charge.

Poisson's Equation

Without spontaneous or piezoelectric polarization, Poisson's equation is

$$\nabla^2\phi = -\frac{\rho}{\epsilon} = -\frac{q}{\epsilon}\left[N_D^+ - N_A^- + N_t^+ - N_t^- + p - n\right] \tag{146}$$

where $N_D^+, N_A^-, N_t^+, N_t^-$ are ionized donor/acceptor densities, and ionized donor/acceptor trap densities, respectively. Also

$$\begin{aligned} \epsilon &= \epsilon_0 \epsilon_r \\ q &= |e| = +1.6\times10^{-19} C \end{aligned} \tag{147}$$

The relative dielectric constant ϵ_r considers the standard electronic plus ionic polarizabilities. When both spontaneous and piezoelectric polarizations are included, the form is as follows.

Start with

$$\nabla \cdot \overline{D} = \rho$$

$$\nabla \cdot \left(\epsilon_0 \overline{E} + \overline{P}\right) = \rho$$

$$\nabla\cdot\left(\epsilon_0\epsilon_r\,\overline{E}+\overline{P}_{\mathrm{PIEZO}}+\overline{P}_{\mathrm{SPON}}\right)=\rho$$

$$\nabla\cdot\left[\epsilon\left(-\nabla\phi\right)\right]+\nabla\cdot\left(\overline{P}_{\mathrm{PIEZO}}+\overline{P}_{\mathrm{SPON}}\right)=\rho$$

$$\epsilon\left[-\nabla^2\phi\right]-\nabla\phi\nabla\epsilon+\nabla\cdot\left(\overline{P}_{\mathrm{PIEZO}}+\overline{P}_{\mathrm{SPON}}\right)=\rho$$

Neglect $\nabla\epsilon$ for simplicity

$$\nabla\epsilon\rightarrow 0 \tag{148}$$

$$\begin{aligned}\nabla^2\phi&=-\frac{\rho}{\epsilon}+\frac{1}{\epsilon}\left(\nabla\cdot\overline{P}_{\mathrm{PIEZO}}+\nabla\cdot\overline{P}_{\mathrm{SPON}}\right)\\&=-\frac{\rho}{\epsilon}-\frac{1}{\epsilon}\left(\rho_b(\mathrm{PIEZO})+\rho_b(\mathrm{SPON})\right)\end{aligned} \tag{149}$$

then

$$\begin{aligned}\nabla^2\phi=&-\frac{q}{\epsilon}\left[N_D^+-N_A^-+N_t^+-N_t^-+p-n\right]\\&-\frac{1}{\epsilon}\left[\rho_b(\mathrm{PIEZO})+\rho_b(\mathrm{SPON})\right]\end{aligned} \tag{150}$$

We see that the potential now also depends on the divergence of the polarizations. Since

$$\overline{P}=d:\vec{\vec{T}}=d:\vec{\vec{\sigma}} \tag{151a}$$

or

$$\overline{P}=e:\vec{\vec{S}}=e:\vec{\vec{u}} \tag{151b}$$

and the components of $\overline{P}$ are linearly related to the components of the stress or strain tensors; an accurate analytical model for the strain variation with position is mandatory.

Schrodinger Equation

Now we consider the effect of the polarization on the energy levels for the 2DEG. Assume the wave functions have the form

$$\psi_j(x,y,z)=\xi_i(z)e^{j\theta_z}e^{jk_1x+jk_2y} \tag{152}$$

then write Schrodinger's equation as

$$-\frac{\hbar^2}{2}\frac{\partial}{\partial z}\left(\frac{1}{m^*}\frac{\partial\xi_i}{\partial z}\right)+\frac{\hbar^2\left(k_1^2+k_2^2\right)}{2m^*}\xi_i+V^*(z)\xi_i=E\xi_i \tag{153}$$

We use an asterisk on the potential energy (PE) term $V^*(z)$, to denote that it represents the total potential energy field that establishes the well. The potential energy near the well is given in figure 8. The figure needs to be discussed in some detail. First, recall the relationships between the electric field $\mathrm{E}(z)$, the electrostatic potential $\phi(z)$ and the electron potential energy band diagram (ref. 43)

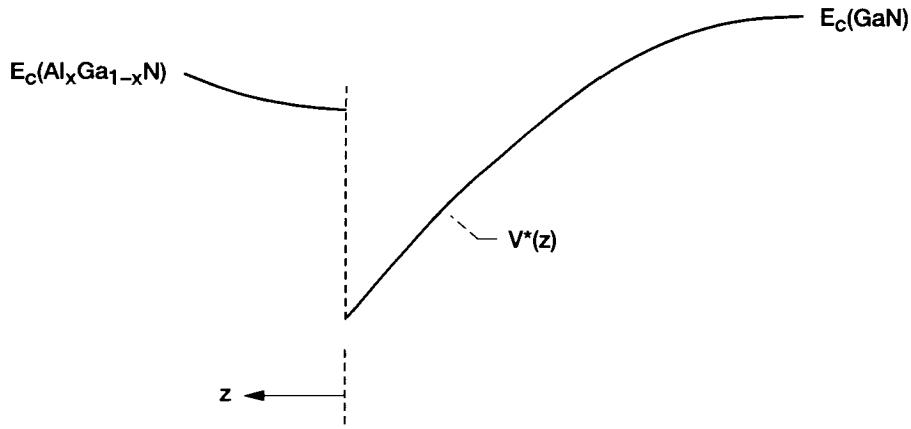

Figure 8.—First-order approximation of potential energy well at heterojunction.

$$\mathrm{E}(z) = -\frac{d}{dz}\phi(z) = \frac{1}{q}\frac{dE_i}{dz} \tag{154}$$

Here $E(z)$ is the magnitude of the component of electric field of interest, and E_i the energy band edge.

Here E_i is a convenient reference energy level, and q is positive as given in equation (147). If only electrostatic forces are considered (the normal case in semiconductors), then the energy band edges take the shape of $\phi(z)$, with the negative sign treated appropriately. For heterojunctions, the band edges and $\phi(z)$ do not track one another. This is due to the differences in electron affinities on either side, and how they change with position as one moves away from the interface. An electric field is generated with a magnitude of $d\chi(z)/dz$. The variation of $\chi(z)$ is difficult to determine thus some standard approximations have been used (ref. 44). Another force field is due to the spatial variation of the density of states (see refs. 45 to 47 for more information). The portion of the well near the notch is assumed to model the entire (or total) potential energy, and as one moves away, the field decreases and reaches flat-band deep into the GaN region. Most authors express $V^*(z)$ as

$$V^*(z) = -e\phi(z) + \Delta E_c U(z) \tag{155}$$

where $U(z)$ is the unit step function. These two terms are sufficient to define the well. The first should include all charges in the vicinity, while the second is of a quantum nature. Another quantum term is the exchange-correlation potential V_{xc}, but it is generally small, and may be neglected. Not all of the charge has been included in equations 146 or 150; namely, that which forms dangling bonds and interface dipoles. Some authors have also included the classic image-force potential. The exchange-correlation is (ref. 48)

$$V_{xc} = -\left[1 + 0.7734x\ln\left(1 + \frac{1}{x}\right)\right]\left(\frac{2}{\pi\alpha r_s}\right)R_y^* \tag{156}$$

where

$$a^* = \frac{4\pi \in_0 \kappa \hbar^2}{m^* q^2} \tag{157}$$

$$\kappa \doteq \in_r (\mathrm{GaN}) \simeq \in_r (\mathrm{Al}_x\mathrm{Ga}_{1-x}\mathrm{N}) \tag{158}$$

$$r_s = r_s(z) = \left[\frac{4\pi}{3}(a^*)^3 n(z)\right]^{-1/3} \tag{159}$$

$$x(z) = \frac{r_s(z)}{21} \tag{160}$$

$$\alpha = \left(\frac{4}{9\pi}\right)^{1/3} \tag{161}$$

$$R_y^* = \frac{q^2}{8\pi \in_0 \kappa a^*} \tag{162}$$

The classic image potential is

$$V_{IM} = \frac{(\kappa_c - \kappa_b)q^2}{16\pi \in_0 \kappa_c(\kappa_c + \kappa_b)|z|} \tag{163}$$

where z is in the channel (GaN). The subscripts c and b stand for channel and barrier (AlGaN) regions.

$$V_{IM} = \frac{(\kappa_c - \kappa_b)q^2}{16\pi \in_0 \kappa_c(\kappa_c + \kappa_b)(-z)} \tag{164}$$

where z is in the barrier ($z > 0$). In practice V_{IM} has been scaled by factors of 0.43, 0.53, and 0.75 for better fits to measured results. The dangling bonds have been represented by the ad hoc term (ref. 49)

$$V_{db} = \frac{q^2}{4\pi \in_0 \in_c d_B} \quad (z < 0, \text{ channel}) \tag{165}$$

where $\in_c = \kappa_c$. The value for d_B is $a_B\sqrt{3}/4$ where a_B is the lattice constant in the barrier. In the barrier

$$V_{db} = \frac{q^2}{4\pi \in_0 \in_b d_B} \quad (z > 0, \text{ barrier}) \tag{166}$$

where $d_c = a_c\sqrt{3}/4$ where a_c is the lattice constant in the channel (GaN region, $z < 0$). Apparently these are special cases of a more general form which varies with position. Assume

$$V_{db}(z) = \frac{n_d q^2}{4\pi \in_0 \in_r (z_0 + |z|)} \tag{167}$$

where n_d is the number of dangling bonds at the interface.

Since the junction is strained, the band gaps on either side will be perturbed via the deformation potential. Write the perturbation as (ref. 50)

$$\Delta E_g(z) = -|a_c|\left[u_{xx}(z) + u_{yy}(z) + u_{zz}(z)\right] \tag{168}$$

where the negative sign reflects the experimental fact that hydrostatic compression ($u_{ii} < 0$) causes the gap to widen. The deformation potential is a_c. Therefore, from the existing literature, the most general expression for $V^*(z)$ is

$$V^*(z) = E_s(z) + \Delta E_g(z) + \Delta E_c u(z) - e\phi(z) + V_{xc}(z) + V_{IM}(z) + V_{dB}(z) \tag{169}$$

where $E_s(z)$ is the conduction band edge (ref. 50). This term is assumed piecewise constant on either side of the junction, and differs by the step height ΔE_c. In effect, it reflects the difference in electron affinities between the two sides. The choice of assuming it is constant with position neglects the field due to $d\chi/dz$ (ref. 44). Only one paper included V_{db} and many neglect V_{xc} and V_{IM} as they are usually small with respect to ΔE_c and $\phi(z)$. Reference 50 is the only one to my knowledge to include $E_s(z)$ and ΔE_g in $V^*(z)$.

The previous paragraphs assumed no interface charge was present, and that $\phi(z)$ is continuous across the interface. However, dipoles may exist at the junction (refs. 46, 51 to 58), and depending on the horizontal mesh size in a simulation, their effects should be included. Consider a 2D dipole formed by nearly adjacent layers of positive and negative charge as shown in figure 9.

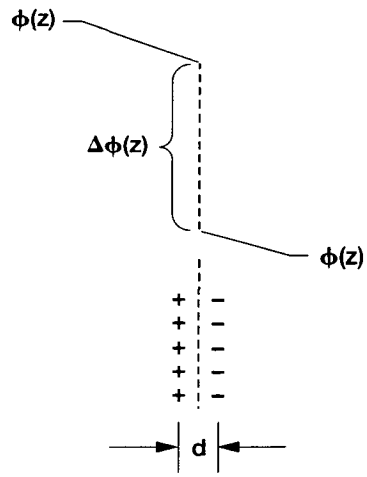

Figure 9.—Discontinuity in potential due to dipole (double layer).

The step change in $\phi(z)$ is (ref. 59)

$$\Delta\phi = \frac{\sigma d}{\epsilon_0} \tag{170}$$

where σ = sheet charge density and d = separation between the sheets.

If the horizontal step size in a simulation is greater than d, then the dipole charge would be overlooked. Equation (170) allows its inclusion without an exceedingly small step (d is on the order of 5 Å). Some heterojunctions have negligible interface dipoles (ref. 58), but this may not be the case for the AlGaN/GaN system. Recall that a dipole (or double layer) is an assembly of charge as indicated above and d is less than other dimensions in the problem. Notice dipoles can add or subtract from ΔE_c depending on their polarity. This may be used to adjust ΔE_c for a given simulation. From experiments, ΔE_c appears to vary from about 0.6 to 2.4 eV. Some of this variation may be due to variations in $\chi(z)$, or doping, but a portion may indeed be due to dipoles.

At the beginning of this section we showed the change in Poisson's equation when polarization was included; now we show how it modifies $V^*(z)$. Rewrite equation (169):

$$V^*(z) = E_s(z) + \Delta E_g(z) + \Delta E_c U(z) - e\phi_n(z) + V_{xc}(z) + V_{IM}(z) + V_{db}(z) + V_{\mathrm{DIPOLE}}(z) - eu_p(z) \tag{171}$$

where we have added two more terms; V_{DIPOLE} and $-eu_p(z)$, the dipole and polarization potentials respectively. It is very important to notice that the $-\phi_n(z)$ now given the subscript n, in equation 171 is that given by equation 146, and not that given in equation 150. We do this to conceptually separate the effects of the normal charges included in Poisson's right hand side, and the image, dangling bond, dipole, and polarization terms.

The potential energy for a dipole is

$$V_{\mathrm{DIPOLE}}(z) = -e\phi_{\mathrm{DIPOLE}} \tag{172}$$

where (ref. 60)

$$\phi_{\mathrm{DIPOLE}} = \frac{\psi_\Omega}{4\pi\epsilon_0\epsilon_r} \tag{173}$$

and $\psi = \sigma_{\mathrm{TOT}} / d\ell$

σ_{TOT} = charge on the positive side of the dipole

$d\ell$ = separation between sheets

Ω = the solid angle subtended by the patch at the observation point (see fig. 10)

Before we introduce polarization effects, recall the definition of the electrostatic potential

$$\phi(\bar{r}) = \frac{1}{4\pi\epsilon_0}\int_{v'} \frac{\bar{\rho}(\bar{r}')dv'}{|\bar{r} - \bar{r}'|} \tag{174}$$

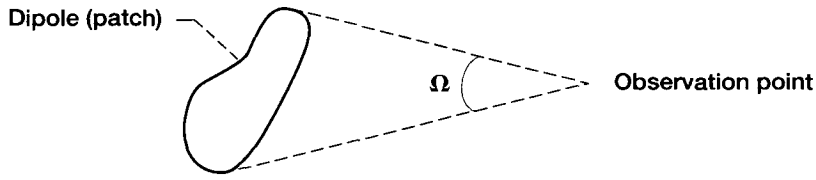

Figure 10.—Geometry for determining potential of finite patch of double layer (dipole).

When a polarization field exists, its potential is (ref. 61)

$$u_P(\bar{r}) = \frac{1}{4\pi \in_0} \int_{v'} \frac{\bar{P}(\bar{r}') \cdot (\bar{r} - \bar{r}')}{|\bar{r} - \bar{r}'|^3} dv' \tag{175}$$

which may be written as

$$\begin{aligned} u_P(\bar{r}) &= \frac{1}{4\pi \in_0} \oint_{s'} \frac{\bar{P} \cdot \overline{ds'}}{|\bar{r} - \bar{r}'|} - \frac{1}{4\pi \in_0} \int_{v'} \frac{\nabla' \cdot \bar{P} dv'}{|\bar{r} - \bar{r}'|} \\ &= \frac{1}{4\pi \in_0} \oint_{s'} \frac{\rho_{sb} ds'}{|\bar{r} - \bar{r}'|} + \frac{1}{4\pi \in_0} \int_{v'} \frac{\rho_{vb} dv'}{|\bar{r} - \bar{r}'|} \end{aligned} \tag{176}$$

where

$$\rho_{sb} = \bar{P} \cdot \hat{n} = P_n \tag{178}$$

$$\rho_{vb} = -\nabla \cdot \bar{P} \tag{179}$$

which are the bound surface and volume charge densities, respectively. The surface integrals are taken over surfaces bounding the polarization distribution.

Now we attempt to ascertain the effects $u_p(\bar{r})$ may have on the final energy levels for the 2DEG via $V^*(z)$. Apparently, the spontaneous polarization has the distribution of surface bound charge density as shown in figure 11.

The values of the charges are (from left to right)

$$-8\times10^{-2} \frac{\mathrm{C}}{\mathrm{m}^2}, 5\times10^{-2} \frac{\mathrm{C}}{\mathrm{m}^2}, \text{ and } 2.9\times10^{-2} \frac{\mathrm{C}}{\mathrm{m}^2}$$

These charges are ρ_{sb} and would contribute to $u_p(\bar{r})$ by the first term in equation 177. Assuming $\nabla \cdot \bar{P}_{\mathrm{SPON}} = 0$, we have no further contributions from $\bar{P}_{\mathrm{SPON}}$. We neglect any pyroelectric terms, as no temperature difference can exist across 4 Å.

For the piezoelectric term, we have

$$\bar{P}_{\mathrm{PIEZO}} = d : \bar{\bar{\sigma}} = e : \bar{\bar{S}} \tag{180}$$

where the stress/strain may be decomposed into residual, thermal, and lattice mismatch components. It can also include stresses due to metal bonding pads. These terms will be dealt with in a later section.

For now, we can say that equation 171 gives the proper potential energy field and one must next evaluate $u_p(\bar{r})$.

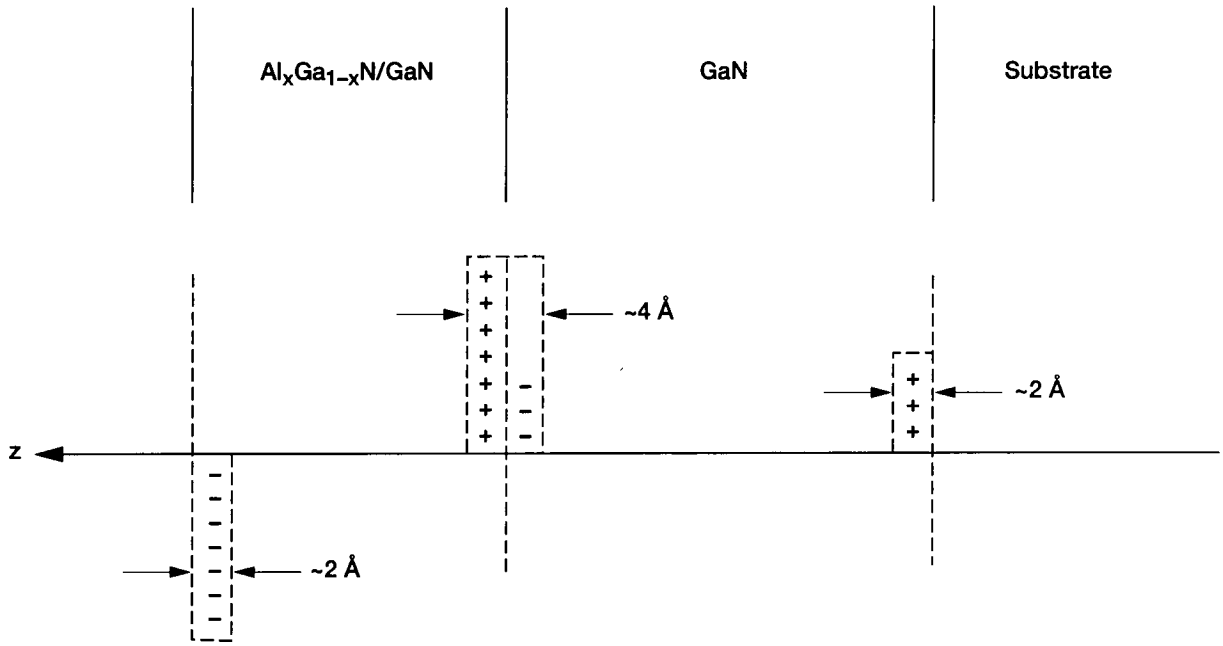

Figure 11.—Assumed bound charge density at three main surfaces of $Al_xGa_{1-x}N/GaN$ substrate HEMT. Charge is assumed to be developed by spontaneous polarization in $Al_xGa_{1-x}N$ and GaN layers.

5. Material Configuration

Figure 12 gives the general layer structure for our device. Our primary goal is to determine the strain at all parts of the structure. Starting at the nucleation layer we treat GaN/AlN/Al_2O_3. The AlN adheres to the sapphire and then allows the GaN to form on its surface. The AlN cracks and forms crystallites (sometimes) during its deposition. The GaN forms threading defects as it nucleates, and these threads spiral up through the material (never stopping) and continue to the AlGaN layer. It is unknown if new ones are initiated and propagate through the AlGaN. The defects have a density between 10^8 and 10^{12} cm^{-2}. The sheet value of $10^{10}cm^{-2}$ corresponds to $2\times10^{17}cm^{-3}$ defects (assuming a sheet 5 Å thick). Figure 13 gives a top view of the 2DEG and the negatively charged threads. The field of a charged thread varies from about 120 V/m to zero in a radius of 10 μm. Perhaps they should be modeled as filled traps; however, there is no obvious way to determine the equivalent trap density.

Eastman's research group at Cornell University state that a Ga face growth along the c-axis is guaranteed if an AlN buffer (nucleation) is used. The GaN is usually in compression and the Al_2O_3 in tension. Figure 14 shows the stress at the interface.

We neglect the fact that sapphire and SiC are piezoelectric, and only consider the strain in the GaN. First of all, the bound positive charge that supports the spontaneous polarization should exist at this interface. Most authors neglect this fact, and implicitly assume the charge is neutralized by immobile negative charge. This may be partially true, but some have noted a conducting channel at this interface. Eastman et al., observe "leakage" at this plane when using SiC and assume it starts to leak due to its relatively small band gap. In our modeling we may assume complete or partial neutralization with fixed charge with the remainder composed of mobile electrons.

Often the strain at the GaN/sapphire interface is assumed to be due to lattice mismatch and/or TEC mismatch. Since the AlN deforms to relieve the ~16 percent lattice mismatch between GaN and sapphire, it is questionable if one can accurately calculate the stress or strain using the misfit parameter method.

Instead, we will use measured in-plane stress and strain. For reference, the misfit parameter for AlN on sapphire is (ref. 5)

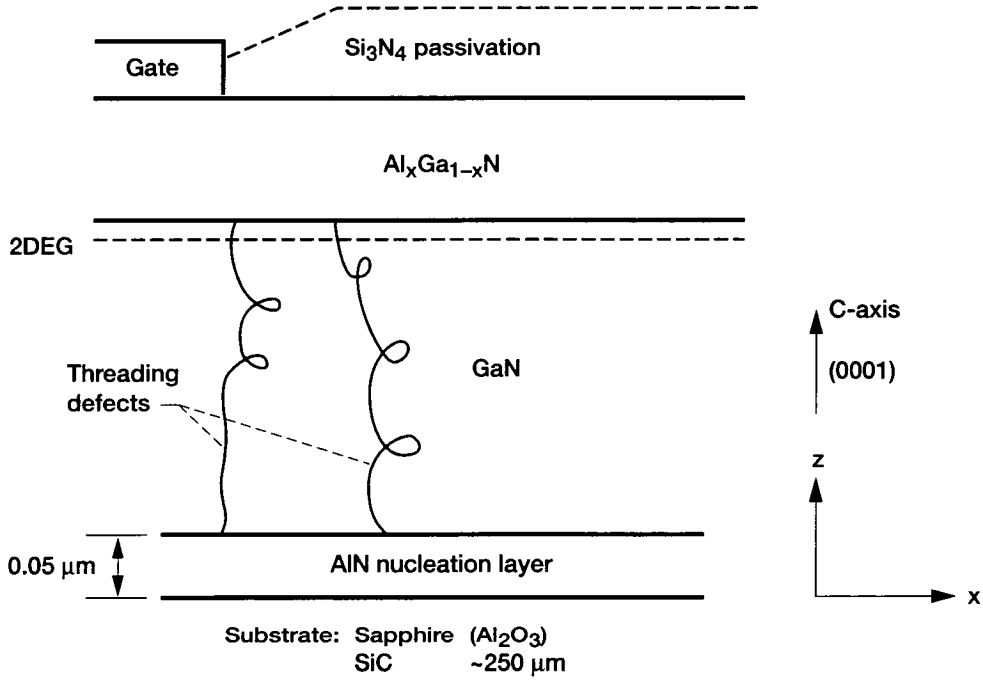

Figure 12.—HEMT structure showing nearly all relevant portions.

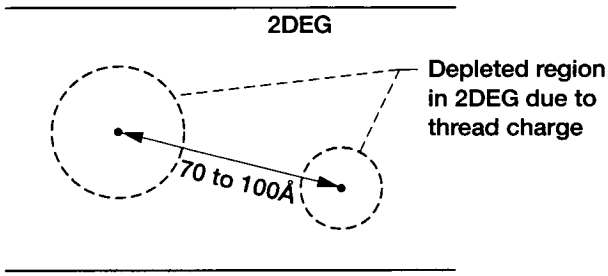

Figure 13.—View looking toward GaN region from $Al_xGa_{1-x}N$ layer. 2DEG is assumed to be uniform with depleted regions around negatively charged threading defects.

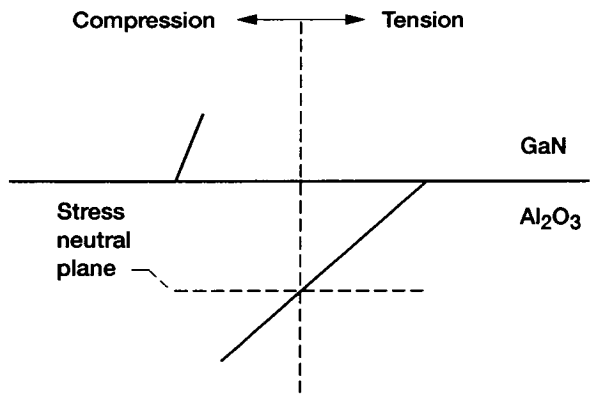

Figure 14.—Approximate stress profile near GaN/sapphire interface.

$$a_0 \quad \mathrm{AlN} = 3.112\ \text{Å} \qquad f_m = \frac{\sqrt{3}(3.112) - 4.7589}{3.112}$$
$$a_0 \quad \mathrm{Al_2O_3} = 4.7589\ \text{Å} \qquad = 20.3\ \text{percent} \tag{181}$$

The $\sqrt{3}$ factor comes about because sapphire is rhombohedral, and the hexagons for the basal plane are rotated 30°. For GaN on AlN we find

$$f_m = \frac{3.1892 - 3.112}{3.1892} = 2.4\ \text{percent}$$
$$\epsilon_{xx} = -f_m = -2.4\ \text{percent} \tag{182}$$

and finally for GaN directly on sapphire we have (c-plane)

$$f_m = \frac{\sqrt{3}(3.1892) - 4.7589}{3.1892} = 24\ \text{percent}$$
or (183)
$$f_m = \frac{\sqrt{3}(3.1892) - 4.7589}{4.7589} = 16\ \text{percent}$$

This latter number is the one most often quoted, however, it is not really appropriate (ref. 5). These are the results from measurements:

For GaN, the in-plane stress (refs. 62 to 65) $\sigma_{xx} = \sigma_{yy} = \sigma_{11}$

$$0.2\ \text{GPa} \le |\sigma_{11}| \le 0.91\ \text{GPa}$$

From reference 15, $|\sigma_{11}| = 0.66 \pm 0.1$ GPa. The lowest and highest values found in literature were

$$|\sigma_{11}|_{\mathrm{LOW}} = 0.18\ \text{GPa}, \quad |\sigma_{11}|_{\mathrm{HIGH}} = 0.91\ \text{GPa}$$

The in-plane strain is $u_{xx} = u_{yy} = u_{11} \equiv \epsilon_{11}$

$$10^{-4} \le |u_{xx}| \le 5 \times 10^{-3}$$

The ranges found, including highest and lowest, are

$$0.058\ \text{percent} \le |u_{zz}| \le 0.125\ \text{percent}, \quad |u_{zz}|_{\mathrm{LOW}} = 0.016\ \text{percent}, \quad |u_{zz}|_{\mathrm{HIGH}} = 0.57\ \text{percent}$$

The calculated thermal stresses are GaN/sapphire $\Delta\alpha = 1.71 \times 10^{-6}$/K $\quad \Delta T \sim 1030$ K

$$\sigma_{TH} = \Delta\alpha \Delta T \frac{300}{1 - 0.25} = 0.7\ \text{GPa} \tag{184}$$

Recall equation 50 of section 1, and repeated after equation 79 reads

$$T_{xx} = -\frac{E}{2\nu} S_{zz} \tag{185}$$

Using the measured σ_{11} and letting E = 300 GPa, we find

$$\in_{zz} = 0.33 \text{ percent}$$

which is within the experimental limits.

For $Al_xGa_{1-x}N$, the measured stress and strains are

$$0.8 \text{ GPa} \le \sigma_{xx} \le 1.4 \text{ GPa}$$
$$0.016 \text{ GPa} \le u_{xx} \le 0.026 \text{ GPa}$$
$$0.0012 \text{ GPa} \le u_{zz} \le 0.0057 \text{ GPa}$$

Moving up through the structure, we may state that the GaN is seldom intentionally doped, however, the minimum n-type carrier density is in the low $10^{17}cm^{-3}$ range. We have discussed the $Al_xGa_{1-x}N$/GaN interface in section 4, and in general, the $Al_xGa_{1-x}N$ is in tensile strain. Most often, authors have assumed the GaN to be fully relaxed, which we will show is not true. The interface between the $Al_xGa_{1-x}N$ and the Si_3N_4 passivation layer has not been reported on extensively, however, it is assumed to play an integral role in the problems presently plaguing the HEMT. It is assumed that the negative charge that supports the spontaneous polarization is neutralized by adsorbed ions. It is also assumed that donors may be present that actually deliver the charge that forms the 2DEG. There is disagreement as to the source of the 2DEG charge. This interface is assumed by some to contain traps that interact with the gate, which causes the unexplained current collapse when radio frequency is applied. Some attribute the collapse phenomena to dielectric loss and bulk traps in the Si_3N_4.

Stress/Strain With Position

This is a most important topic, but unfortunately, not discussed much in the literature. Only one reference, Demarest (ref. 62), used the standard software package for stress/strain from ANSYS. The paper shows the strain variation around metal pads on SiO_2 layers. It should be mentioned that when GaN is grown on sapphire and SiC with AlN nucleation layers, polymorphs of Wz and zincblende regions may coexist. In some cases as much as 25 percent may be zincblende (on an Si wafer). During growth the GaN is in tension, but during cooling it goes into compression in the basal plane. Misfits form during the entire process, so the state of strain is highly variable from sample to sample due primarily to the different temperatures for growth, cooldown rates, and other factors.

For reference, the basal plane strains at an interface are

$$\in_{xx} = \in_{yy} = \pm f_m = \pm \frac{a_0 - a_{SUB}}{a_{SUB}} \tag{186}$$

where a_{SUB} is the lattice constant in the layer in which the strain is sought. The corresponding strain along the c-axis is

$$\epsilon_{zz} = -2\frac{c_{13}}{c_{33}}\epsilon_{xx} \tag{187}$$

For GaN, $c\downarrow$ and $a\uparrow$, that is, as c decreases, a increases. The net strain is the combination of lattice mismatch, thermal mismatch (TEC), and residual strain. The latter often dominates, so we should rely on measured results as much as possible. For thin layers (up to about 2 μm), we may assume the stress is linear (ref. 63). Figure 15 depicts the measured stress for films of GaN on 6H-SiC (by MOCVD). In the region near 2 μm the material apparently relaxes and remains in horizontal tension for further growth.

In figure 16 from (ref. 64), which shows the biaxial stress $\sigma_{xx} = \sigma_{yy} = \sigma_{11}$ to be negative (compression).

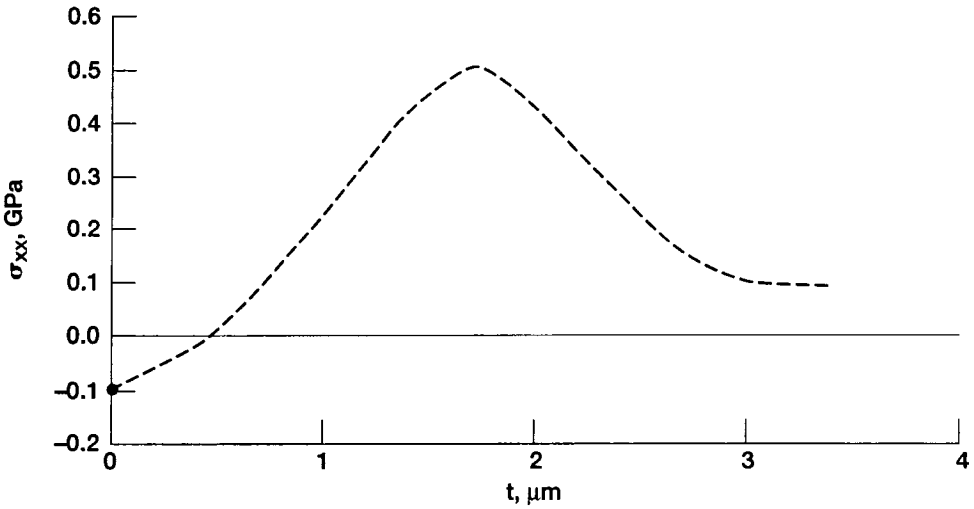

Figure 15.—Measured stress in GaN epilayer grown on 6H-SiC by MOCVD. Note, stress-free region occurs near 0.5 μm thickness (see ref. 66).

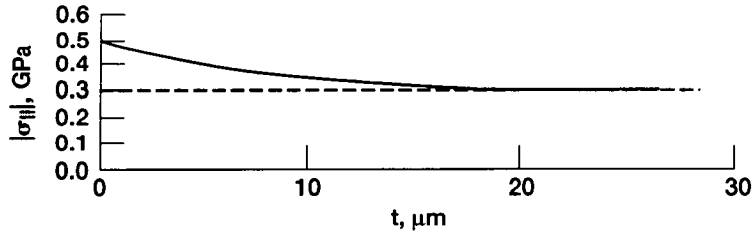

Figure 16.—Reduction in stress with thickness of GaN on sapphire. Here $\sigma_{xx} = \sigma_{yy} \equiv \sigma_{||}$ which is negative (film in compression). Absolute value is plotted.

This trend is common; GaN on sapphire is often in compression while on SiC it is in tension. This, however, is not necessary, and the films may be in either state of strain on both substrates. It all depends on the mode, and temperature of growth, the nucleation layer preparation, the thickness of both the nucleation layer and the GaN layer, and the crystal orientation of the substrate and its surface condition.

For GaN on sapphire (Al_2O_3), it appears that the strain decreases with thickness to some power, or almost linearly, or exponentially from the AlN layer (refs. 14, 65, 66). Table X gives the vertical strain with thickness t in μm (ref. 65).

TABLE X.—STRAIN ALONG THE c-AXIS VERSUS FILM THICKNESS

t, μm	Strain	Fit equation result
1	12.3	12.3
5	7.3	7.3
20	4.6	4.66
60	1.5	3.26

The fit equation is

$$\epsilon_{zz} = \left[12.3 \times 10^{-4}\right] t^{-0.32416} \tag{188}$$

Table XI gives the basal plane compressive stress versus thickness (ref. 14), and it looks almost linear.

TABLE XI.—MEASURED STRESS VERSUS FILM THICKNESS FROM REF. 14

μm	Compressive stress, GPA
1	−0.64
10	−0.59
20	−0.56
50	−0.47

The paper by Detchprohm (ref. 67) shows the vertical (c-axis) strain varies exponentially from the nucleation surface. The strain does not relax until the layer is about 100 μm thick. This data was taken with MOCVD and HVPE grown samples (see fig. 17).

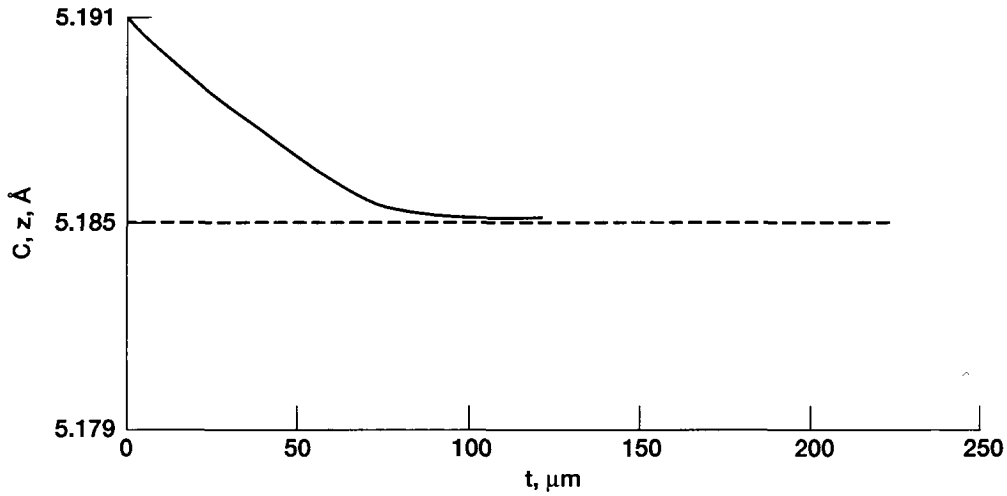

Figure 17.—Relaxation of c-axis strain for GaN on sapphire.

The c-axis lattice constant was fitted to an exponential

$$c(z) = 5.185 + (0.006)e^{-0\,0692} \quad c \text{ in Å}, z \text{ in } \mu \tag{189}$$

then the strain with position is

$$\epsilon_{zz} = \frac{c(z) - 5.185}{5.185}$$
$$\epsilon_{zz} = \frac{0.006}{5.185} e^{-0.0692} \tag{190}$$

$$\frac{\frac{\Delta c}{c}}{\frac{\Delta a}{a}} = \frac{2s_{13}}{s_{11} + s_{12}} \tag{191}$$

For Si_3N_4

$$-1.2\,\text{GPa} \le \sigma_{11} \le -0.02\,\text{GPa}$$

6. Band-Gap Issues

The band diagram in figure 18 gives the ideal charge distributions at the Schottky barrier, the AlGaN/GaN interface, and the nucleation/substrate plane.

We show positive charge on the Schottky barrier metallization that accumulates to neutralize the negative charge of the spontaneous polarization. The positive polarization charge and the 2DEG are shown at the heterojunction, and the spontaneous charge with some form of neutralization is shown at the nucleation layer. This is the minimum charge distribution for the device. Figure 19 shows the charge distributions for dipoles and dangling bonds that may exist at the $Al_xGa_{1-x}N$/GaN interface.

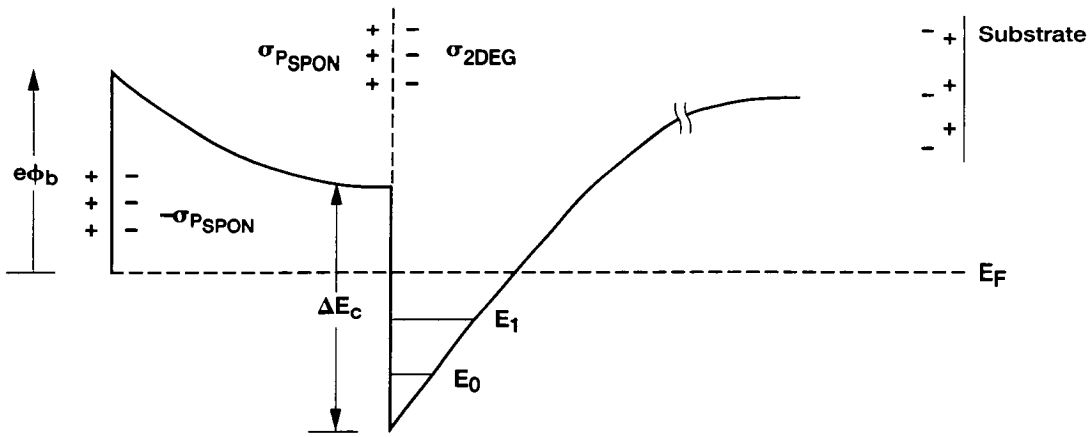

Figure 18.—Minimum charge distribution for an $Al_xGa_{1-x}N$ GaN HEMT. Charge at Schottky barrier, heterojunction, and GaN/substrate interface shown left to right.

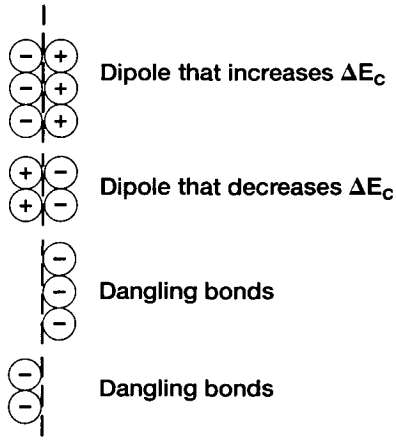

Figure 19.—Detail of possible charge conditions at heterojunction.

The charge state in the $Al_xGa_{1-x}N$ and the Si_3N_4 passivation layer are not considered here. The $Al_xGa_{1-x}N$ barrier contains Al, but the total charge there is unknown. Often an Si donor layer is placed a few hundred angstroms from the interface to provide the 2DEG carriers. This doping apparently has a strong effect on the strain state of the barrier, which is a significant source of piezoelectric charge.

We can omit the step discontinuity in ϕ given in equation 170 of section 4, by combining it with the step; that is, $e\Delta\phi + \Delta E_c = \Delta E_c'$. This keeps ϕ continuous, if that causes problems with the software solvers. While this is convenient, it eliminates the force field of the dipole in the Schrodinger equation. Recall that the step ΔE_c is due to the absence of available states in the barrier region, and not some form of repulsive field due to charge. The dangling bonds do not cause a jump in ϕ and pose no problem.

The range of ΔE_c reported in the literature is about

$$0.17\,\text{eV} < \Delta E_c < 1.8\,\text{eV} \tag{192}$$

Anderson's model assumes

$$\Delta E_c = \left| \chi_{Al_xGa_{1-x}N} - \chi_{GaN} \right| \tag{193}$$

However the uncertainties in χ are very large (refs. 68 and 69)

For GaN $2.1 < \chi < 4.26$ eV (194)

For $Al_xGa_{1-x}N$ $\chi(x) = 3 - 4x$ for $x < 0.75$
or $= 3.25 - 2.95x$ $x < 0.75$ (195)

The steps in the band edges have been reported to be as follows

$$\begin{aligned}\Delta E_v &= 0.78x \text{ eV} \\ &= 0.81\ (x = 1) \text{and no strain}\end{aligned} \tag{196}$$

$$\text{also} \quad 0.2 < \Delta E_v < 1.4 \text{ eV}$$

For the nucleation sequence of $GaN/AlN/Al_2O_3$

$$\begin{aligned}\Delta E_v &= 0.57 \pm 0.22 \text{ eV} \quad \text{for 5 to 20 Å layers} \\ &= 0.7 \pm 0.24 \text{ eV} \\ &= 0.8 \pm 0.3 \text{ eV}\end{aligned} \tag{197}$$

From these and knowing the band gaps, the step in E_c is known. For the following range

$$0.15 < \Delta E_c < 0.56 \text{ eV}$$

the step is

$$\Delta E_c(x) = 0.75\left[E_g(\text{Al}_x\text{Ga}_{1-x}\text{N}) - E_g(\text{GaN})\right] \doteq 1.96x \tag{198}$$

For strain-free GaN, the following have been reported (see ref. 70)

$$\Delta E_v = 1.36 \pm 0.07 \qquad \frac{\Delta E_c}{\Delta E_v} = \frac{52}{48} \quad \text{or} \quad \frac{\Delta E_c}{\Delta E_v} = \frac{65}{20} \tag{199}$$

Thus, ΔE_c is a fitting factor, and unfortunately it is one of the dominant terms in $V^*(z)$. Next we consider the change in $E_g(z)$ with strain. We write

$$E_g(\text{STRAINED}) = E_g(\text{BULK}) \pm \Delta E_g \tag{200}$$

where E_g (bulk) means the unstrained/undoped material. The change may be expressed as

$$\Delta E_g = \sum D_{ij}\, \epsilon_{ij} \tag{201}$$

where D_{ij} is the deformation tensor and ϵ_{ij} is the strain tensor. For GaN

$$D_1 = -0.88,\ D_2 = 4.52,\ D_3 = 5.4,\ D_4 = -2.7,\ D_5 = -2.85,\ D_6 = 3.82 \text{ eV} \tag{202}$$

A simpler form using in-plane stress $\sigma_{xx} = \sigma_{yy}$ is

$$\Delta E_g = \frac{\partial E_G}{\partial \sigma_{11}} \sigma_{11} \tag{203}$$

where $\partial E_g/\partial \sigma_{11}$ = 21 to 27 meV/GPa
= 42 meV/GPa for hydrostatic stress (and Si doped)

Sometimes one finds (ref. 71)

$$\frac{dE_g}{d\ \text{Pressure}} = 42\ \text{meV/GPa} \tag{204}$$

Other forms using both in-plane and c-axis strains are as follows:

$$E_g(\text{STRAINED}) = E_g(\text{RELAXED}) \pm \left|\frac{\partial E_g}{\partial \epsilon_{zz}}\right| \left|\epsilon_{zz}\right| \tag{205}$$

where

$$\frac{\partial E_g}{\partial \epsilon_{zz}} = D_3 - D_4 \frac{c_{33}}{c_{13}} \tag{206}$$

	GaN	AlN
D_3 (eV)	5.8	8.84
D_4 (eV)	−3.25	−3.92

Another form from Yang (ref. 72) is

$$\Delta E_g = \Delta E_{\text{HYDRO}} + \Delta E_{\text{SHEAR}} \tag{207a}$$

$$\Delta E_{\text{HYDRO}} = -a\left[\epsilon_{xx} + \epsilon_{yy} + 2\epsilon_{zz}\right] \tag{207b}$$

$$\Delta E_{\text{SHEAR}} = -b\left[\epsilon_{xx} + \epsilon_{yy} - 2\epsilon_{zz}\right] \tag{208}$$

where a = −8.16 eV, and b = 3.71 eV. In some cases the hydrostatic and uniaxial strains are given by

$$\epsilon_{\text{HYDRO}} = \frac{2}{3}\left(\epsilon_{11} + \frac{\epsilon_{\perp}}{2}\right)$$

$$\epsilon_{\text{UNIAX}} = \frac{1}{3}\left(\epsilon_{\perp} - \epsilon_{11}\right) \tag{209}$$

$$\text{along}\,[0001]$$

Another form is

$$\Delta E_g = C\,\epsilon_{zz} \tag{210}$$

where C was determined by experiment to be 12 eV.

Finally, one finds in terms of stress

$$\left|\frac{\partial E_g}{\partial \epsilon_{zz}}\right| = 10.1 - 15.4 \text{ eV} \tag{211}$$

in terms of strain

$$\begin{aligned} \frac{\partial E_g}{\partial \epsilon_{11}} &= -6.1 \text{ eV} && \epsilon_{11} \le 0.0032 \\ &= -8.2 \text{ to } -13 \text{ eV} && \text{(TENSILE)} \\ &= -16 \text{ eV} && \epsilon_{11} > 0.0032 \end{aligned} \tag{212}$$

The expression for ΔE_g in equation 168 in section 4 is that due to hydrostatic stress only.

In figure 20 (based on a figure in the literature); we show the energy gap of GaN with in-plane strain. Some authors claim that the curve is symmetrical, that is, the gap increases for both compression and tension.

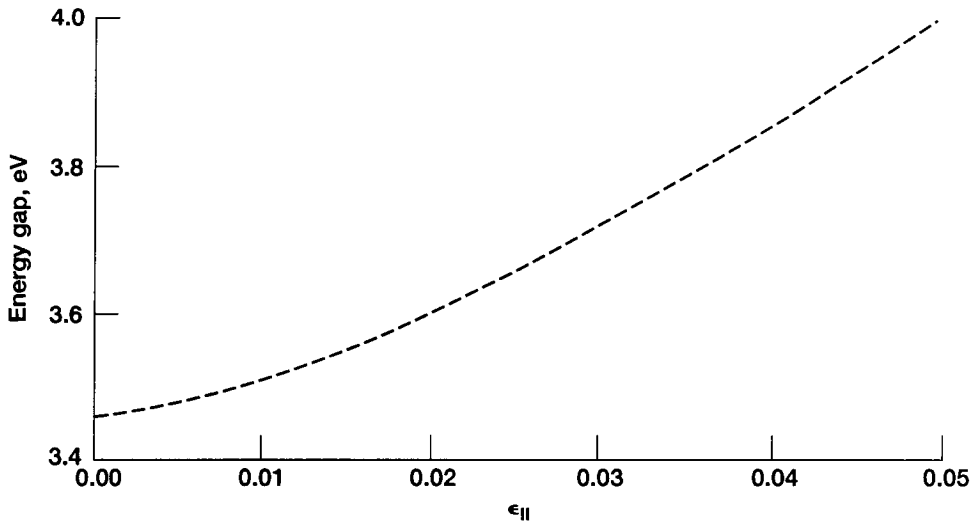

Figure 20.—Variation of bandgap of GaN with basal plane strain $\epsilon_{II} = \epsilon_{xx} = \epsilon_{yy}$ (see ref. 73).

Now we consider the change in band gaps with temperature (refs. 73 to 75).

For GaN

$$\begin{aligned} E_g &= 3.503 + 5.08 \times 10^{-4} \frac{T^2}{T - 996 \text{ K}} \text{ eV} \\ \text{or } E_g &= 3.509 - 7.32 \times 10^{-4} \frac{T^2}{T + 700 \text{ K}} \text{ eV} \\ \text{or } E_g &= E_g(T = 0) - 8.32 \times 10^{-4} \frac{T^2}{T + 836 \text{ K}} \text{ eV} \end{aligned} \tag{213}$$

For AlN

$$E_g = 6.118 - 1.8\times10^{-3}\frac{T^2}{T+1462\,\mathrm{K}}\,\mathrm{eV}$$
$$E_g(x,T) = (3.42x + 0.068) - 8.73\times10^{-4}\frac{T^2}{T+830\,\mathrm{K}}eV \tag{214}$$

The band gap of $Al_xGa_{1-x}N$ is assumed to vary with mole-fraction x as

$$E_g(x) = x\,E_g(\mathrm{AlN}) + (1-x)E_g(\mathrm{GaN}) - bx(1-x) \tag{215}$$

where the bowing parameter "b" varies from 0.53 to 2.6 eV in the literature. Some have even stated it is 0, ±0.2, or ±0.3 eV. The following forms are found.

$$\begin{aligned} E_g &= 3.43 + 2x + 0.7x^2 \\ &= 3.43 + 2.56x \end{aligned} \tag{216}$$

7. Thermal Conductivity

Let $\kappa(T_0)$ be the thermal conductivity at T_0 (normally 20 °C). Then the variation with temperature is

$$\kappa(T) = \kappa(T_0)\left(\frac{T}{T_0}\right)^{-r}\frac{\mathrm{W}}{\mathrm{cm\ K}} \tag{217}$$

TABLE XII.—SUMMARIZES THE VALUES FOR OUR MATERIALS

Material	κ	r
Sapphire	0.25 to 0.50	0.544
SiC	3.3 SI, 0.5	0.524
GaN	1.3 to 1.7	
Si_3N_4	0.37	
AlN	2.0	
Si	2.0	

Some experimental results for AlN are below.

TABLE XIII.—THERMAL CONDUCTIVITY VARIATION WITH TEMPERATURE FOR AlN

T	Experimental value for κ
300	2.85
400	1.80
600	0.96
1000	0.48

8. Orders of Magnitude of Terms and Approximations

The exact form for the potential of a rectangle of charge is given in the appendix. It is tedious so we will assume the potential of a disc of charge is a reasonable approximation. The potential of a disc of radius "a" is

$$\phi(z)=\frac{\sigma_0}{2\epsilon_0\epsilon_r}\left[\sqrt{a^2+z^2}-z^2\right] \tag{218}$$

where σ_0 is the surface charge density. Assume the source-drain spacing is 2 μm, then $a = 1$ μm. For the spontaneous polarization at the interface, the effective charge density is

$$\sigma_0 = 5.1\times10^{-2}\frac{\mathrm{C}}{\mathrm{m}^2} \tag{219}$$

Evaluate at 70 Å from the surface

$$\phi(70\,\text{Å})=320\,\mathrm{V} \tag{220}$$

This would be the value if no screening existed due to mobile charge. We will assume the screening can be modeled using the classic Debye-screening factor

$$f_{DS}=e^{-z/\ell_D} \tag{221}$$

where ℓ_D is the Debye length

$$\begin{aligned}\ell_D &= \sqrt{\frac{\epsilon kT}{2\rho_0 q}}\\ \rho_0 &= n_0 q = 1.6\times10^6\frac{\mathrm{C}}{\mathrm{m}^3}\end{aligned} \tag{222}$$

The densities in the 2DEG are on the order of 10^{19} cm^{-3}, which yields a length of about 8.25 Å. The evaluating point of 70 Å is then about 8.5 Debye lengths, and the reduction factor becomes

$$f_{DS}=2\times10^{-4} \tag{223}$$

Thus, the potential is 64 mV, which is well within acceptable limits.

Now we estimate the terms in equation 171 in section 4, to ascertain their relative magnitudes. The step in the conduction band is bounded as

$$0.17\,\mathrm{eV}\le\Delta E_c\le1.8\,\mathrm{eV} \tag{224}$$

Therefore, all the other terms should be less than an eV or so. The change in the bandgap due to strain, ΔE_g, has a large dispersion. From section 6, we find

$$20\,\mathrm{meV}\le\Delta E_g\le230\,\mathrm{meV} \tag{225}$$

While large, it is definitely within acceptable limits. For the electrostatic potential, we start with the electric field from equation 129 of section 2. Its value is 4.8×10^8 V/m, which is about 100 times larger than that for GaAs. It is very near the breakdown value (5 to 6×10^8 V/m). At 70 Å we have

$$\phi(70\text{Å}) = E_s(0)(70\text{Å}) = (4.8\times10^8\ \text{V/m})(70\times10^{-10}\,\text{m}) \\ = 3.36\ \text{V} \qquad \therefore e\phi = -3.36\ \text{eV} \tag{226}$$

which is high. If we reduce the field by a factor of 10, which is reasonable, then the value is acceptable. There are two justifications for the reduction by the factor of 10; one is the uncertainty in the stiffness parameters while the other is the chosen order of magnitude of the strain. The exchange correlation is –38.6 meV and the image force gives –0.146 meV. The dangling bond gives

$$V_{db} = 20.7 n_d \quad \text{meV} \tag{227}$$

where n_d is the number of bonds. This would give a very large value for even one bond. Using the screening factor reduces it by 10^{-4}, which brings it into a reasonable range. The dipole contribution gives –896 eV without screening (for just 100 electrons on a sheet). The screening reduces it to –89.6 meV, which is excellent.

Now we estimate some of the strains that will contribute to Poisson's equation 150 in section 4. We start with the strains due to metal pads and dielectric films on the $Al_xGa_{1-x}N$ top surface. Consider a semi-infinite film of thickness h on a substrate. The stresses due to this "single edge" (refs. 76 and 77) (see fig. 21).

$$T_1 = \sigma_{xx} = \frac{-2f_E}{\pi}\left(\frac{x_1^3}{r_1^4}\right) \tag{228}$$

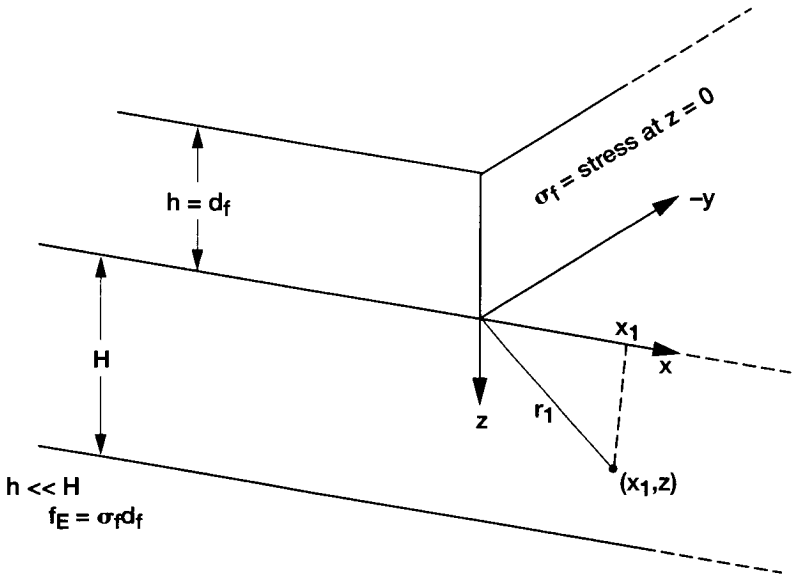

Figure 21.—Geometry for calculation of stress in region z ≥ 0. Single stage at x = 0 develops stresses for x ≥ 0.

$$T_2 = \sigma_{yy} = \frac{-2\nu f_E}{\pi}\left(\frac{x_1}{r_1^2}\right) \tag{229}$$

$$T_3 = \sigma_{zz} = \frac{-2 f_E}{\pi}\left(\frac{x_1 z^2}{r_1^4}\right) \tag{230}$$

$$T_4 = \sigma_{yz} = 0 \tag{231}$$

$$T_5 = \sigma_{xz} = \frac{-2 f_E}{\pi}\left(\frac{x_1^2 z}{r_1^4}\right) \tag{232}$$

$$T_6 = \sigma_{xy} = 0 \tag{233}$$

These are correct for $x > 0$. They are not correct for large negative x (which is out of our range). When two edges are used we have the following situation (see fig. 22).

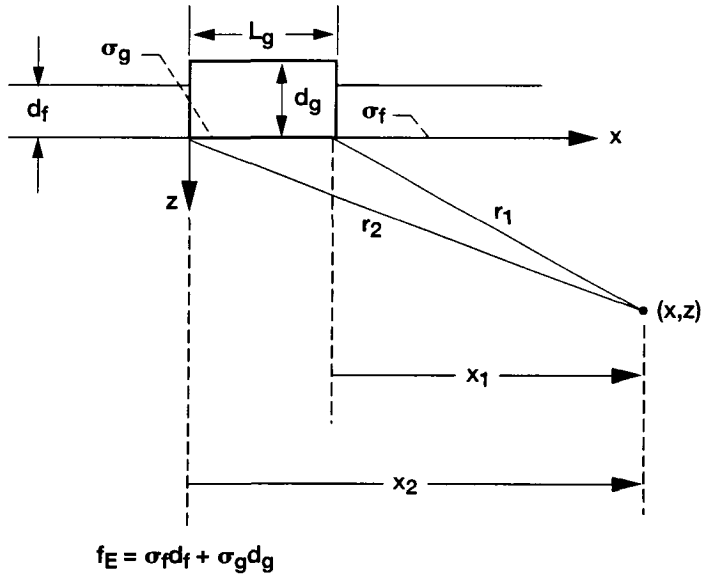

Figure 22.—Geometry for loading due to pad of width L_g. Modeled as superposition of two single edges at x = 0 and x = L_g.

$$f_E = \sigma_f d_f + \sigma_g d_g \tag{234}$$

where σ_f, σ_g are stresses produced at $z = 0$.

$$T_1 = \sigma_{xx} = -\frac{2 f_E}{\pi}\left(\frac{x_1^3}{r_1^4} - \frac{x_2^3}{r_2^4}\right) \tag{235}$$

$$T_2 = \sigma_{yy} = -\frac{2\nu f_E}{\pi}\left(\frac{x_1}{r_1^2} - \frac{x_2}{r_2^2}\right) \tag{236}$$

$$T_3 = \sigma_{zz} = -\frac{2f_E}{\pi}\left(\frac{x_1 z^2}{r_1^4} - \frac{x_2 z^2}{r_2^4}\right) \tag{237}$$

$$T_4 = \sigma_{yx} = 0 \tag{238}$$

$$T_5 = \sigma_{xz} = -\frac{2f_E}{\pi}\left(\frac{x_1^2 z}{r_1^4} - \frac{x_2^2}{r_2^4}\right) \tag{239}$$

$$T_6 = \sigma_{xy} = 0 \tag{240}$$

This is known as the "effective edge" model. For $Al_xGa_{1-x}N$ or GaN we have

$$\begin{bmatrix} P_1 \\ P_2 \\ P_3 \end{bmatrix} = \begin{bmatrix} 0 & 0 & 0 & 0 & d_{15} & 0 \\ 0 & 0 & 0 & d_{15} & 0 & 0 \\ d_{31} & d_{31} & d_{33} & 0 & 0 & 0 \end{bmatrix} \begin{bmatrix} T_1 \\ T_2 \\ T_3 \\ T_4 \\ T_5 \\ T_6 \end{bmatrix} \tag{241}$$

$$P_1 = d_{15} T_5 \tag{242}$$

$$P_2 = 0 \tag{243}$$

$$P_3 = d_{31}(T_1 + T_2) + d_{31} T_3 \tag{244}$$

then

$$P_x = d_{15}\left(\frac{-2f_E}{\pi}\right)\left(\frac{x_2^2 z}{r_2^4} - \frac{x_1^2 z}{r_1^4}\right) \tag{245}$$

$$P_y = 0 \tag{246}$$

$$P_z = d_{31}\left(\frac{2f_E}{\pi}\right)\left(\frac{x_1^3}{r_1^4} - \frac{x_2^3}{r_2^4}\right) + d_{31}\left(\frac{2rf_E}{\pi}\right)\left(\frac{x_1}{r_1^2} - \frac{x_2}{r_2^2}\right) + d_{33}\left(\frac{2f_E}{\pi}\right)\left(\frac{x_1 z^2}{r_1^4} - \frac{x_2 z^2}{r_2^4}\right) \tag{247}$$

Notice the coordinate system is not that used in other sections. To conform to that system observe the following changes: z (here) goes to $(-z)$ there, and y (here) goes to $(-y)$ there. Thus, the only changes required are the signs of y and z. This has already been done in equations 245 and 247 above.

A previous study using the above equations has been done in the $Al_xGa_{1-x}As/GaAs$ heterojunction system (ref. 78). It was observed that the stress changed from tension to compression at the mole-fraction $x = 0.03$. The crystal type was zincblende (cubic) so

$$\begin{bmatrix} P_1 \\ P_2 \\ P_3 \end{bmatrix} = \begin{bmatrix} 0 & 0 & 0 & e_{14} & 0 & 0 \\ 0 & 0 & 0 & 0 & e_{14} & 0 \\ 0 & 0 & 0 & 0 & 0 & e_{14} \end{bmatrix} \begin{bmatrix} u_{11} \\ u_{22} \\ u_{33} \\ u_{44} \\ u_{55} \\ u_{66} \end{bmatrix} \tag{248}$$

Note, only shearing stresses cause $\overline{P}$ in this system. If grown in the [100] direction, then $\overline{P} = 0$; if grown in any other direction, then $\overline{P} \neq 0$. For GaAs

$$\nu = 0.23$$

$$d_{14} = 2.6 \times 10^{-10} \frac{\text{cm}}{\text{V}} \quad \text{(close to GaN)} \tag{249}$$

$$P_x = d_{14}\sigma_{zx}$$

$$P_y = d_{14}\sigma_{yz} \tag{250}$$

$$P_z = \tfrac{1}{2} d_{14}\left(\sigma_{yy} - \sigma_{xx}\right) \tag{251}$$

Figure 23 shows qualitatively the differences between the "edge" model and a more accurate calculation using ANSYS (ref. 79). Figure 24 is from (ref. 80), which shows the piezoelectric charge near a gate pad. Observe the charge density oscillates from positive to negative as one traverses the device on a horizontal line. The densities are as large as 10^{17} cm^{-3}, which is the same order of magnitude as the background density obtained in GaN.

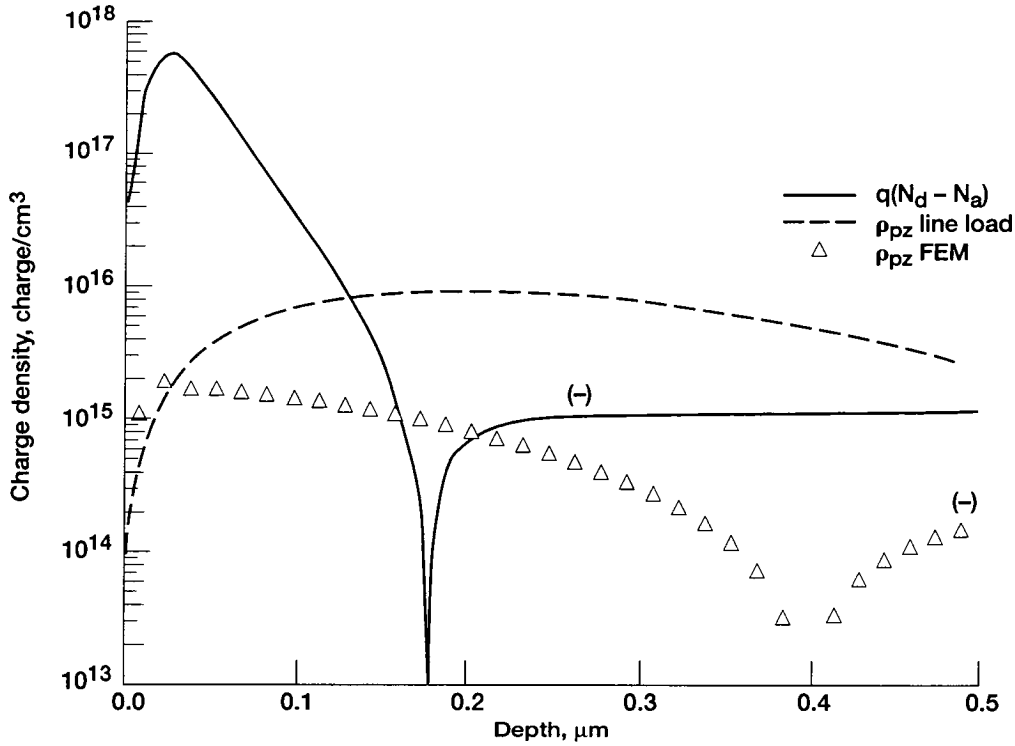

Figure 23.—Doping profile and piezoelectric charge density ρ_{pz} calculated by "edge" load line method, and more accurate ANSYS finite element method (FEM) solution.

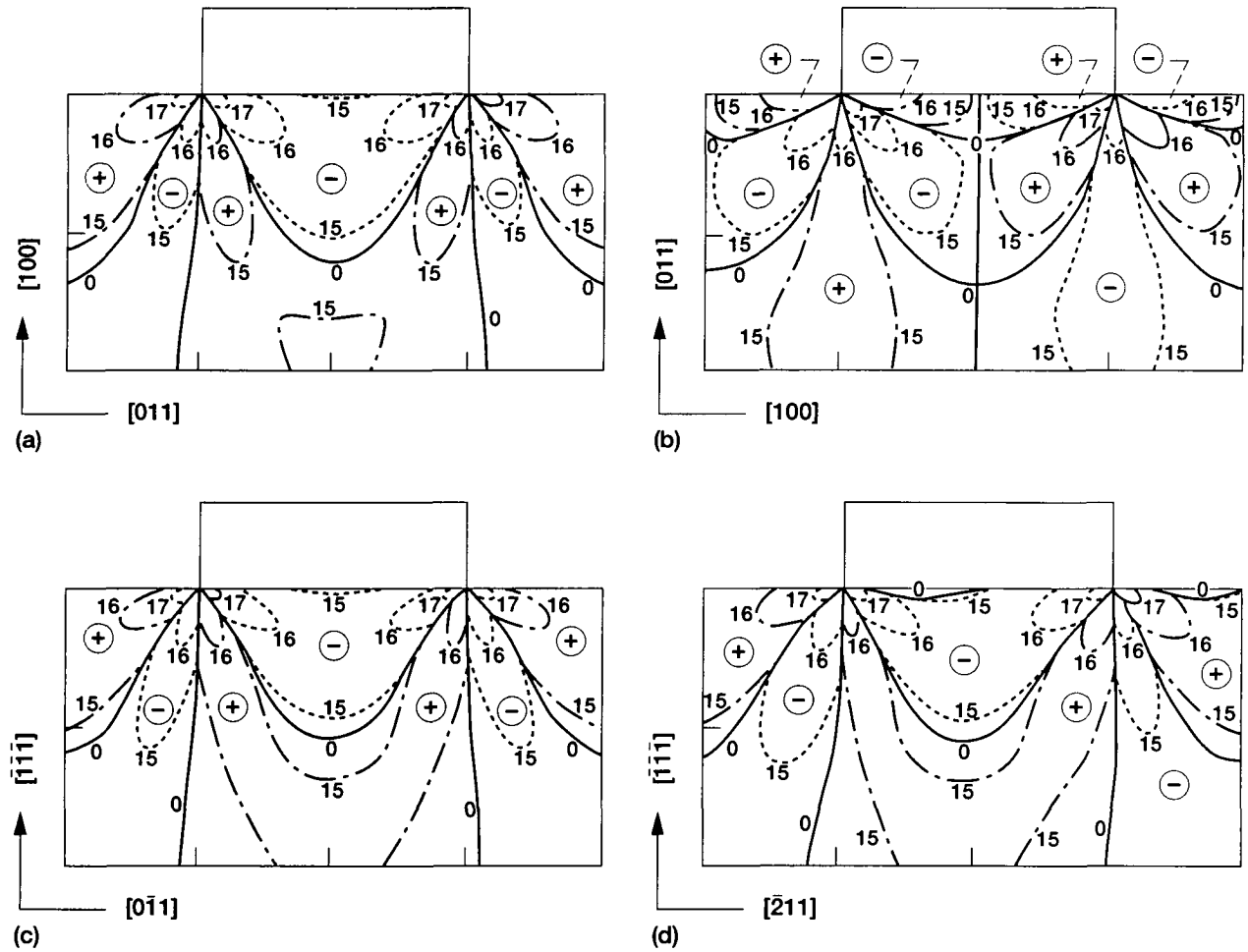

Figure 24.—Characteristic "bifoleum loops" of piezoelectric charge generated by edges of pad on surface. Numbers represent charge density; 17 means $10^{17}cm^{-3}$. (a) [0$\bar{1}$1]-oriented field-effect transisters (FET) on [100] plane. (b) [0$\bar{1}$1]-oriented FET on [011] plane. (c) [2$\bar{1}\bar{1}$]-oriented FET on [$\bar{1}\bar{1}\bar{1}$] Ga plane. (d) [0$\bar{1}$1]-oriented FET on [$\bar{1}\bar{1}\bar{1}$] Ga plane.

9. Heterojunctions

In other sections various properties about heterojunctions were mentioned. This section seeks to gather much of the information I have gathered that may prove useful. First of all, the assumption that the interface strain is equal to that of the misfit parameter needs to be discussed. While it may serve as a guide, its reliability is questionable. First of all, the intrinsic and thermal strain components must also be calculated to estimate the strain at a junction. The most common interface is that of GaN on sapphire. The misfit parameters in GaN and sapphire are

For GaN $$f_m = \frac{3.189\sqrt{3} - 4.7589}{3.189} = 24 \text{ percent}$$

For sapphire $$f_m = \frac{3.189\sqrt{3} - 4.7589}{4.7589} = 16 \text{ percent} \qquad (252)$$

It would appear that the GaN would be in lateral tension (and thus in vertical compression), and visa-versa for the sapphire. Experimentally, while GaN is growing on sapphire, it is in tension. The corresponding TEC are

For GaN $\alpha = 5.59\times10^{-6}/\mathrm{K}$

For sapphire $\alpha = 7.3\times10^{-6}/\mathrm{K}$

This implies the GaN would be in compression. Theory would say the thermal stress is

$$\begin{aligned}|\sigma_{11}| &= \Delta\alpha\Delta T\frac{E(\mathrm{GaN})}{1-\nu}\\ &= \left(1.71\times10^{-6}\right)(1020)\frac{320}{1-0.25}\,\mathrm{GPa}\\ &= 0.74\ \mathrm{GP}a\end{aligned} \tag{253}$$

Experimentally, the net stress is near 0.66 GPa, compression.

The next combination is AlN on sapphire (which is the standard nucleation layer). The misfit parameters are

For AlN $$f_m = \frac{|3.189-4.7589|}{3.112} = 53\ \text{percent}$$

For sapphire $$f_m = \frac{|3.112-4.7589|}{4.7589} = 35\ \text{percent} \tag{254}$$

The TEC for sapphire is $a = 7.3\times10^{-6}/°\mathrm{C}$. It would appear that the AlN is in lateral tension latticewise and compression from TECs.

Next we consider GaN/AlN

$$f_m = \frac{3.189-3.112}{3.189} = 2.4\ \text{percent}, \qquad f_m = \frac{3.189-3.112}{3.112} = 2.5\ \text{percent} \tag{255}$$

The GaN should be in lateral compression latticewise but in tension from the TECs. When joined, the measured lattice is 3.184 Å. Experimentally, the GaN is in compression.

For GaN/6H-SiC

$$\begin{aligned}f_m &= \frac{3.189-3.08}{3.189} = 3.4\ \text{percent}\\ \alpha(6\mathrm{H}-\mathrm{SiC}) &= 4.2\times10^{-6}/°\mathrm{C}\end{aligned} \tag{256}$$

The GaN in compression latticewise and tension TEC-wise. In many experiments it is in tension, from 0.1 to 0.2 GPA (for 3-μm films).

For GaN/4H-SiC

$$f_m = \frac{|3.189 - 4.23|}{3.189} = 33 \text{ percent}$$
$$\alpha(4H - SiC) = 4.2 \times 10^{-6}/°C \tag{257}$$

Both imply tension for GaN.

The case for $Al_xGa_{1-x}N$/GaN, the lattice constant for $Al_xGa_{1-x}N$ is

$$A(x) = (-.077x + 3.189)\text{Å} \tag{258}$$

Then its misfit parameter on GaN is

$$f_m = \frac{-0.077x + 3.189 - 3.189}{-0.077x + 3.189} \tag{259}$$

The TEC for AlN is about 5.3, as compared to GaN's 5.59, so assume no added strains during cooling. Experimentally, $Al_xGa_{1-x}N$ is in tension. The in-plane stress is between 0.82 and 1.33 GPa. The in-plane strain $\in_{11}$ is between 0.016 and 0.026. Table XIII gives the vertical strain with mole-fraction

TABLE XIII.—THE VERTICAL STRAIN WITH MOLE-FRACTION IN $Al_xGa_{1-x}N$

x	0.05	0.1	0.15	0.20	0.25
$\in_{zz}$ (percent)	0.12	0.24	0.35	0.48	0.57

The c-axis lattice constant in GaN is

$$C(x) = (-0.2667x + 5.17)\text{Å} \quad 0 < x < 0.9 \tag{260}$$

The total spontaneous polarization is

$$\overline{P}_{SPON}(x) = -0.029(1 - x) - 0.081x \ \frac{C}{m^2}$$
$$= (-0.029 - 0.052x) \Rightarrow 3.25x \ (10^{13}) \text{ electrons/cm}^2 \tag{261}$$

$$\overline{P}(\text{PIEZO})\ \text{GaN} = 0.0163x \frac{C}{m^2} \tag{262}$$

$$\overline{P}(\text{total})\ \text{GaN} = P_{SPON}(GaN) + P_{PIEZO}(\text{GaN})$$
$$= (-0.029 + 0.0163x) \frac{C}{m^2} \tag{263}$$

$$P_{\text{PIEZO}}\left(\text{Al}_x\text{Ga}_{1-x}\text{N}\right) = 4.26x\left(10^{-2}\right)\frac{\text{C}}{\text{m}^2}$$
$$= (2.66-3)(x)\left(10^{13}\right)\text{electrons/cm}^2 \tag{264}$$
$$= 2\left[e_{31}(x) - e_{33}(x)\frac{c_{13}(x)}{c_{33}(x)}\right]$$

$$P\,(\text{total})(\text{both materials}) = \left(-8.4x - 1.9x^2\right)\times 10^{-6}\ \frac{\text{C}}{\text{m}^2}$$
$$\doteq -0.096x\ \frac{\text{C}}{\text{m}^2} \tag{264a}$$

$$2.6\times 10^{-2} < P(\text{total}) < 4\times 10^{-2}\ \frac{\text{C}}{\text{m}^2} \tag{265}$$

The stiffness coefficients are

$$c_{13}(x) = 5x + 103 \doteq 11x + 105\ \text{GPa} \tag{266}$$

$$c_{33}(x) = -32x + 405\ \text{GPa} \tag{267}$$

The stress coefficients are (refs. 5, 81, 82)

$$e_{31}(x) = -0.11x - 0.49\ \frac{\text{C}}{\text{m}^2} \tag{268}$$

$$e_{33}(x) = -0.73x + 0.73\ \frac{\text{C}}{\text{m}^2} \tag{269}$$

The relative dielectric constant is

$$\kappa(x) = -0.5x + 9.5 \tag{270}$$

The Schottky barrier heights are (ref. 83)

$$e\phi_b = (1.3x + 0.84)\text{eV} \qquad \text{Ni} \tag{271}$$

$$e\phi_b = (2.44x + 0.91)\text{eV} \qquad \text{Ti/Al} \tag{272}$$

The effective masses are

$$m_e(x) = [0.3x + 0.2(1-x)]m_0 \tag{273}$$

$$m_{hh}(x) = [3.53x + 1.76(1-x)]m_0 \tag{274}$$

The electric field is

$$\varepsilon(x) = \left(7.9\times10^{-4} + 1.15\times10^{7}\,x\right)\text{V/cm} \tag{275a}$$

$$\text{or } \varepsilon(x) = \left(9.5x + 2.1x^{2}\right)\times10^{6}\ \text{V/cm} \tag{275b}$$

$$\text{or } \varepsilon(x) = 1.2x\times10^{6}\ \text{V/cm} \tag{275c}$$

Finally, the surface sheet density is

$$\sigma_{TOT}(x) = 0.068x\ \frac{\text{C}}{\text{m}^2} \tag{276}$$

$$n_s(x) = 6x\times10^{12}\ \frac{\text{e}}{\text{cm}^2} \tag{277a}$$

$$\text{or } n_s(x) \doteq 5.5x\times10^{13}\ \frac{\text{e}}{\text{cm}^2} \tag{277b}$$

10. Defects

For unintentionally doped AlGaN the carrier density is near 1.0^{17}cm^3. The carriers are assumed to be caused by N vacancies, but there is no general agreement. Listed are some speculations on defects.

1. Surface traps cause the radio frequency compression. These are emptied and filled by the gate voltage. Some speculate that the gate voltage alters the strain in the barrier and passivation layers and thus the amount of trapped charge.
2. Shallow traps cause I-V dc current loops.
3. Deep traps in the buffer are the cause for the I-V dc current collapse. Hot electrons are introduced into the buffer for drain voltages above 20 V. Gate voltages have no effect on this process.

A surface donor at 1.4 eV, 1.65 eV.
A deep trap at 1.91 eV.
A shallow trap at .95 to 1.0 eV with capture cross-section $4\times10^{-12}\,\text{cm}^2$.
For mole-fractions, the density of these traps are:

TABLE XIV.—APPROXIMATE TRAP DENSITY IN $Al_xGa_{1-x}N$

x	N, cm^{-3}
0.05	5×10^{17}
0.15	2×10^{18}
0.25	5×10^{18}

For semi-insulating (SI) GaN a trap exists at 2.15 eV below E_c with density between 3×10^{9} and $3\times10^{10}\,\text{cm}^{-2}$. For normal GaN, traps at 1.8 and 2.85 eV below E_c. A deep acceptor trap exists at 2.2 eV below E_c with density $\sim1\times10^{10}\,\text{cm}^{-2}$.

The nitrogen vacancy has a state 40 meV below E_c, and the E_2 trap exists 0.55 eV below E_c. The trap that causes dc current collapse is 1.19 eV above E_V. The dominant Mg trap is 150 to 200 meV above E_V. A trap exists at 0.95 eV above E_V and the characteristic yellow emission is due to a transition between levels 1 eV below E_c to one 0.2 eV above E_V. The following list gives the levels (I assume with respect to E_V) of many of the standard impurities found in GaN (ref. 22).

Zn	0.34, 1.8–1.9, 2.2, 2.5–2.6, 2.8
Mg	0.25, 2.95, 3.2 (note, 0.15 to 0.2 in the paragraph above)
Cd	0.55, 2.7, 2.85
Be	0.7, 2.2
Hg	0.41, 2.9, 2.43
C	0.86, 2.15
Li	0.75, 2.23
P	2.85
As	2.58
Si	0.225

11. Amplifiers

The best ever performance: 9.1 W/mm at 10 GHz on 4H-SiC (refs. 84 to 86). The maximum available is 12 W/mm, for then the channel goes above 300 °C and/or the SiC substrate starts to leak, and large anomalous current starts.

Devices have been plagued by both dc and tuning-induced failures.

Eastman says degrade most theoretical f_t by 30 percent. SiC has maximum thermal dissipation of 27.8 W/mm, but starts leaking at 10.9 W/mm. SiC leaks more than sapphire due to smaller bandgap.

Eastman $0.2 < x < 0.4$

Channel temperature < 300 °C

P(max) at 10 GHz = 12.5 W/mm

The channel temperature is

$$T_{\text{CHANNEL}} = T_0(\text{SUBSTRATE}) + R_{th} I_D V_{DS}$$

$$R_{th} = 24\left[1 + (T - T_0)\times 10^{-3}\right]\frac{\text{K}\cdot\text{mm}}{\text{W}}$$

$$T_{\text{CHANNEL}}\,(\text{MAX}) = 500\ \text{K}$$

The devices are predominantly thermally limited, so thermal simulations would be important.

Appendix

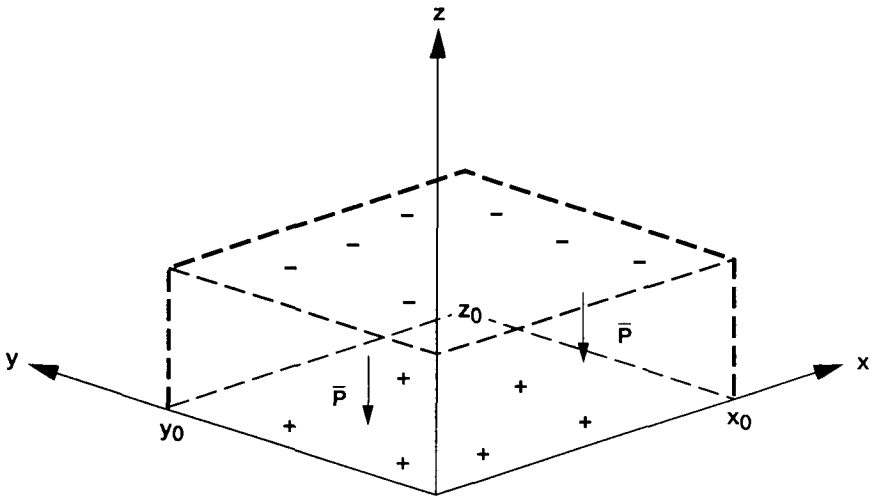

Figure 25.—Epitaxial $Al_xGa_{1-x}N$ layer ($z \geq 0$) on GaN ($z \leq 0$) with spontaneous polarization $\bar{P}$ and bound charge on plane $z = 0$ and $z = z_0$.

The field due to the spontaneous polarization of the epitaxial layer of $Al_xGa_{1-x}N$ is developed. Figure 25 gives the geometry. The spontaneous polarization is specified by

$$P_{SPON} = -P_0 \bar{a}_z \tag{A1}$$

Where $P_0 = 0.08$ C/m^2 on the top surface and 0.051 C/m^2 on the bottom surface. This assumes no neutralization of the negative charge on the top surface due to adsorbed charge. It also models the net charge at the heterojunction. Starting with the first term of equation 176 of section 4

$$u_p(\bar{r}) = \oint_{s'} \frac{\bar{P} \cdot \hat{n}\, ds'}{4\pi \in_0 |r - r'|} \tag{A2}$$

On the upper surface $\hat{n} = \bar{a}_z$, so $\bar{P} \cdot \hat{n} = -P_0$. While on the lower surface we have $\hat{n} = -\bar{a}_z$, $\bar{P} \cdot \hat{n} = P_0$. Thus, the two surfaces at $z = 0$ and $z = z_0$ are just uniform charge sheets.

On the lower surface we have

$$\bar{r}' = x'\bar{a}_x + y'\bar{a}_y \tag{A3}$$

$$\bar{r} = x\bar{a}_x + y\bar{a}_y + z\bar{a}_z \tag{A4}$$

$$|\bar{r} - \bar{r}'| = \sqrt{(x - x')^2 + (y - y')^2 + z^2}\; ds' = dx'dy' \tag{A5}$$

Using elementary steps and reference 87 we find

$$u_p(\bar{r}) = \int_0^{x_0} \int_0^{y_0} \frac{1}{4\pi \in_0} \frac{P_0 dy' dx'}{\left[(x-x')^2 + (y+y')^2 + z^2\right]^{1/2}} \tag{A6}$$

From no. 200.01 (reference 87), we have

$$\begin{aligned} u_p(\bar{r}) = {} & \frac{-P_0}{4\pi \in_0} \int_0^{x_0} \ell n\left[(y-y_0) + \sqrt{(y-y_0)^2 + A^2}\right] dx' \\ & + \frac{P_0}{4\pi \in_0} \int_0^{x_0} \ell n\left[y + \sqrt{y^2 + A^2}\right] dx' \end{aligned} \tag{A7}$$

where

$$A^2 = (x-x')^2 + z^2 \tag{A8}$$

Now for the first integral in equation (A7)

$$\begin{aligned} u_p(\bar{r}) = {} & \frac{-P_0}{4\pi \in_0} \ell n\left[(y-y_0) + \sqrt{(x_0-x)^2 + (y-y_0)^2 + z^2}\right] \\ & + \frac{P_0}{4\pi \in_0} \ell n\left[(y+y_0) + \sqrt{x^2 + (y-y_0)^2 + z^2}\right] \\ & + \frac{P_0}{4\pi \in_0} \left\{ \sqrt{\nu^2 + b\nu - z^2} + \frac{b}{2} \ell n \left| 2\sqrt{\nu^2 + b\nu - z^2} + 2\nu + b \right| - z \sin^{-1} \left| \frac{b\nu - 2z^2}{|\nu| \sqrt{b^2 + 4z^2}} \right| \right\}_{\nu_a}^{\nu_b} \end{aligned} \tag{A9}$$

where $b = 2(y_0 - y)$ and $y \le y_0$ always

$$\nu_b = (y-y_0) + \sqrt{(x_0-x)^2 + z^2 + (y-y_0)^2}$$

$$\nu_a = (y-y_0) + \sqrt{x^2 + z^2 + (y-y_0)^2}$$

where we have used 380.311, 261.01, 380.001, and 380.111 from reference 87. The second term of equation (A7) is the negative of equation (A9) with $y_0 = 0$.

On the upper surface we have

$$\bar{r}' = x'\bar{a}_x + y'\bar{a}_y + z_0\,\bar{a}_z \tag{A10}$$

$$\bar{r} = x\bar{a}_x + y\bar{a}_y + z\bar{a}_z \quad |\bar{r} - \bar{r}'| = \left[(x-x')^2 + (y-y')^2 + (z-z_0)^2\right]^{1/2} \tag{A11}$$

$$ds' = dx'\,dy' \tag{A12}$$

then

$$u_p(\bar{r}) = \frac{-P_0}{4\pi \in_0} \int_0^{x_0} \int_0^{y_0} \frac{dy'dx'}{\left[(x-x')^2 + (y-y')^2 + (z-z_0)^2\right]^{1/2}} \tag{A13}$$

By observation of equation (A6), we see equation (A13) only differs by a negative sign and the replacement of z^2 with $(z-z_0)^2$; thus only minor modifications are necessary on equation (A9), to evaluate equation (A13). The superposition of the results of equation (A9) and (A13) constitute the complete potential of the two sheets of charge. The valid range is $y_0 \leq y$, and all x and z.

References

1. B.A. Auld, *Acoustic Waves and Fields in Solids (volumes I and II)*, John Wiley, 1973.
2. J.F. Nye, *Physical Properties of Crystals*, Oxford, Clarenden Press, 1957.
3. C. Deger, et al., "Sound velocity of AlGaN thin films obtained by surface acoustic-wave measurements," Applied Physics Letters (APL), 71, p. 2400, 1998.
4. M. Eickhoff and O. Ambacher, "Piezoresistivity of $Al_xGa_{1-x}N$ layers and $Al_xGa_{1-x}N$/GaN heterostructures," Journal of Applied Physics (JAP), 90 p. 3383, 2001.
5. O. Ambacher, et al., "Two dimensional electron gases induced by spontaneous and piezoelectric polarization in undoped and doped AlGaN/GaN heterostructures," JAP, 87, p. 334, 2000.
6. A. Polian, et al., "Elastic constants of gallium nitride," JAP, 79, p. 3343, 1996.
7. R. Schwarz, et al., "Elastic moduli of gallium nitride," APL, 70, p.1122, 1997.
8. B. Foutz, http://iiiv.tn.cornell.edu/www/foutz/nitride.html
9. Hughes and Gaylord, *Basic Equations of Engineering Science*, Schaum's Outline Series, McGraw-Hill, 1964.
10. C. Kisielowski, et al., "Strain-related phenomena in GaN thin films," Phys. Rev. B, 54, p. 17745, 1996.
11. N. Maeda, et al., "Two-dimensional electron-gas density in AlGaN/GaN heterostructure field-effect transistors," APL 73, p.1856, 1998.
12. E. Etzkorn and D. Clarke, "Cracking of GaN films," JAP, 89, p. 1025, 2001.
13. B. Skromme, et al., "Strain determination in heteroepitaxial GaN," APL, 71, p. 829, 1997.
14. T. Kozawa, et al., "Thermal stress in GaN epitaxial layers grown on sapphire substrates," JAP, 77, p. 4389, 1995.
15. S. Hearne, et al., "Stress evolution during metalorganic chemical vapor deposition of GaN," APL, 74, p. 356, 1999.
16. M. Mynbaeva, et al., "Strain relaxation in GaN layers grown on porous GaN sublayers," MRS Inter. Jour. Nitride Semicond. Res. 4, 14, 1999.
17. G. Olsen and M. Ettenberg, "Calculated stresses in multilayered heteroepitaxial structures," JAP, 48, p. 2543, 1977.
18. N. Itoh, et al., "Study of cracking mechanism in GaN/α-Al_2O_3 structure," JAP, 58, p. 1828, 1985.
19. S. Pearton, et al., "GaN Electronics," Advanced Materials, 12, p. 1571, 2000.
20. H. Morkoc, et al., "Polarization effects in nitride semiconductor device structures and performance of modulation doped field effect transistors," Solid-State Electronics, 43, p. 1753, 1999.
21. H. Morkoc, et al., "GaN-based modulation doped FETs and UV detectors," Solid-State Electronics, 46, p. 157, 2002.
22. H. Morkoc, et al., "Large-band-gap SiC, III-V nitride, and II-VI ZnSe-based semiconductor device technologies," JAP, 76, p. 1363, 1994.
23. W. Cady, *Piezoelectricity,* McGraw-Hill, 1946.
24. H. Jaffe and D. Berlincourt, "Piezoelectric Transducer Materials," Proc. IEEE, 53, p. 1372, 1965.
25. S. Muensit, et al., "Shear piezoelectric coefficients of gallium nitride and aluminum nitride," APL, 75, p. 3965, 1999.
26. A. Wright, "Elastic properties of zinc-blende and wurtzite AlN, GaN, and InN," JAP, 82, p. 2833, 1997.
27. P. Ramvall, et al., "Influence of a piezoelectric field of the electron distribution in a double GaN/$Al_xGa_{1-x}N$ heterojunction," APL, 74, p. 3866, 1999.
28. J. Im, et al., "Reduction of oscillator strength due to piezoelectric fields in GaN/$Al_xGa_{1-x}N$ quantum wells," Phys Rev B, 57, p. R9435, 1998.
29. A. Durelli, E. Phillips, and C. Tsao, *Introduction to the Theoretical and Experimental Analysis of Stress and Strain,* McGraw-Hill, 1958.

30. F. Bernardini, et al., "Spontaneous polarization and piezoelectric constants of III-V nitrides," Phys. Rev. B, 56, p. R10 024, 1997.
31. F. Bernardini and V. Fiorentini, "Polarization-Based Calculation of the Dielectric Tensor of Polar Crystals," Phys. Rev. Lttrs., 79, p. 3958, 1997.
32. F. Bernardini and V. Fiorentini, "Macroscopic polarization and band offsets at nitride heterojunctions," Phys. Rev. B, 57, p. R9427, 1998.
33. F. Bernardini and V. Fiorentini, "Spontaneous Versus Piezoelectric Polarization in III-V Nitrides: Conceptual Aspects and Practical Consequences," Phys. Status Solidi, (b) 216, p. 391, 1999.
34. F. Bernardini and V. Fiorentini, "Polarization fields in nitride nanostructures: 10 points to think about," Applied Surface Science, 166, p. 23–29, Oct. 9, 2000.
35. O. Ambacher, et al., "Role of Spontaneous and Piezoelectric Polarization Induced Effects in Group-III Nitride Based Heterostructures and Devices," Phys. Status Solidi, (b), 216, p. 381, 1999.
36. J. Garrido, et al., "Polarization Field Determination in AlGaN/GaN HFETs," Phys. Status Solidi, (a), 176, p. 195, 1999.
37. R. Resta, "Macroscopic polarization in crystalline dielectrics," Rev. Mod. Phys., 66, p. 899, 1994 (see p. 912).
38. A. Hangleiter, "Optical properties and polarization fields in the nitrides," J. of Luminescence, 87–89, p. 130, 2000 (see p. 132).
39. R. Martin, "Piezoelectricity," Phys. Rev. B, 5, p. 1607, 1972 (see p. 1611).
40. S. Park, et al., "Comparison of zinc-blende and Wurtzite GaN semiconductors with spontaneous polarization and piezoelectric field effects," JAP, 87, p. 353, 2000.
41. Fafara, et al., "Collective and Molecular Modes in Ferroelectric and Antiferroelectric Liquid Crystals," IEEE Trans. Dielectrics and Electrical Insulation, 8, p. 477, 2001.
42. F. Sacconi, et al., "Spontaneous and Piezoelectric Polarization Effects on the Output Characteristics of AlGaN/GaN Heterojunction Modulation doped FETs," IEEE Trans. Electron Devices, 48, p. 450, 2001.
43. B. Streetman, *Solid State Electronic Devices*, Prentice Hall, 1990, p. 115.
44. W. Liu, *Handbook of III-V Heterojunction Bipolar Transistors*, John Wiley, p. 127, 1998.
45. M. Lundstrom and R. Schuelke, "Modeling Semiconductor Heterojunctions in Equilibrium," Solid-State Electronics, 25, p. 683, 1982.
46. A. Chatterjee and A. Marshak, "Theory of Abrupt Heterojunctions in Equilibrium," Solid-State Electronics, 24, p. 1111, 1981.
47. A. Marshak and K. van Vliet, "Electrical Current in Solids With Position-Dependent Band Structure," Solid-State Electronics, 21, p. 417, 1978.
48. F. Stern and S. Sarma, "Electron energy levels in GaAs-$Ga_{1-x}Al_x$ As heterojunctions," Phys Rev B, 30, p. 840, 1984.
49. H. Unlu and A. Nussbaum, "Band Discontinuities as Heterojunction Device Design Parameters," IEEE Trans. Electron Devices, 33, p. 616, 1986.
50. Jogai, "Free electron distribution in AlGaN/GaN heterojunction field-effect transistors," JAP, 91, p. 3721, 2002.
51. L. Van Ruyven, et al., "Optical Phenomena in Ge-GaP Heterojunctions," Solid-State Electronics, 8, p. 631, 1965.
52. W. Harrison, "Elementary theory of heterojunctions," J. Vac. Sci. Tech., 14, p. 1016, 1977.
53. R. Grant, et al., "Observation of the Orientation Dependence of Interface Dipole Energies in Ge-GaAs," Phys. Rev Lttrs, 40, p. 656, 1978.
54. W. Frensley and H. Kroemer, "Theory of the energy-band lineup at an abrupt semiconductor heterojunction," Phys. Rev B, 16, p. 2642, 1977.
55. G. Baraff, et al., "Self-Consistent Calculation of the Electronic Structure at an Abrupt GaAs-Ge Interface," Phys Rev Lttrs, 38, p. 237, 1977.

56. W. Pickett, et al., "Ge-GaAs (100) Interface: A Self-Consistent Calculation of Interface States and Electronic Structure," Phys Rev Lttrs, 39, p. 109, 1977.
57. J. Donnelly and A. Milnes, "The Capacitance of p-n Heterojunctions Including the Effects of Interface States," IEEE Trans. Electron Devices, 14, p. 63, 1967.
58. H. Stormer, et al., "Two-Dimensional Electron Gas at a Semiconductor-Semiconductor Interface," Solid-State Comm., 29, p. 705, 1979.
59. W. Hauser, *Introduction to the Principles of Electromagnetism*, Addison-Wesley, p. 125, 1971.
60. W. Smythe, *Static and Dynamic Electricity 2nd Ed.*, p. 14, McGraw-Hill, 1950.
61. J. Reitz and F. Milford, *Foundations of Electromagnetic Theory*, Addison-Wesley, p. 70, 1960.
62. Demarest, et al., "Nanoscale characterization of stresses in semiconductor devices by quantitative electron diffraction," APL, 77, p. 412, 2000.
63. N. Edwards, et al., "Trends in residual stress for GaN/AlN/6H-SiC heterostructures," APL 73, p. 2808, 1998.
64. E. Valcheva, et al., "Elimination of nonuniformities in thick GaN films using metalorganic chemical vapor deposited GaN templates," JAP, 90, p. 6011, 2001.
65. Reynolds, et al., "Strain variation with sample thickness in GaN grown by hydride vapor phase epitaxy," JAP, 88, p. 1460, 2000.
66. W. Li, et al., "Residual strain in GaN epilayers grown on sapphire and (6H)SiC substrates," APL, 68, p. 2705, 1996.
67. T. Detchprohm, et al., "Relaxation Process of the Thermal Strain in the GaN/-Al O Heterostructure and Determination of the Intrinsic Lattice Constants of GaN Free From the Strain," Japanese JAP, p. L1454, 1992.
68. S. Grabowski, et al., "Electron affinity of $Al_xGa_{1-x}N$ (0001) surfaces," APL 78, p. 2503, 2001.
69. P. Bridger, et al., "Measurement of induced surface charges, contact potentials, and surface states in GaN by electric force microscopy," APL, 74, p. 3522, 1999.
70. M. Nardelli, et al., "Strain effects on the interface properties of nitride semiconductors," Phys Rev B, 55, p. R7323, 1997.
71. P. Perlin, et al., "Pressure studies of gallium nitride: Crystal growth and fundamental electronic properties," Phys. Rev. B, 45, p. 13307, 1992.
72. T. Yang and M. Kim, "Screening and strain effects on the ground-state energy of quasi-two-dimensional quantum well system," JAP, 89, p. 1156, 2001.
73. Z. Yang and Z. Xu, "Electronic and optical properties of unstrained and strained Wurtzite GaN," Phys. Rev. B, 54, p. 17577, 1996.
74. T. Zheleva, "Thermal mismatch stress relaxation via lateral epitaxy in selectively grown GaN structures," APL, 74, p. 2492, 1999.
75. R. Passler, "Parameter Sets Due to Fittings of the Temperature Dependencies of Fundamental Bandgaps in Semiconductors," Phys. Status Solidi, (b) 216, p. 975, 1999.
76. S. Wong, et al., "Analytic solution of stress distribution under a thin film edge in substrates," APL, 79, p. 1628, 2001.
77. S. Hu, "Film-edge-induced stress in silicon substrates," APL, 32, p. 5, 1978.
78. P. Asbeck, et al., "Piezoelectric Effects in GaAs FET's and Their Role in Orientation-Dependent Device Characteristics," IEEE Trans. Electron Devices, 31, p. 1377, 1984.
79. J. Ramirez, et al., "Development and Experimental Verification of a Two-Dimensional Numerical Model of Piezoelectrically Induced Threshold Voltage Shifts in GaAs MESFET's," IEEE Trans. Electron Devices, 35, p. 1232, 1988.
80. T. Onodera and H. Nishi, "Theoretical Study of the Piezoelectric Effect on GaAs MESFET's on (100), (011), and (111) Ga, and (111) As Substrates," IEEE Trans. Electron Devices, 36, p. 1580, 1989.
81. Danielsson, et al., "The influence of band offsets on the IV characteristics for GaN/SiC heterojunctions," Solid State Electronics, 46, p. 827, 2002.

82. Guy, et al., "Extensional piezoelectric coefficients of gallium nitride and aluminum nitride," APL, 75, p. 4133, 1999.
83. Ponce, et al., "Spatial distribution of the luminescence in GaN thin films," APL, 68, p. 57, 1996.
84. L. Eastman, et al, "High Frequency AlGaN/GaN MODFET's," MRS Inter. Jour. Nitride Semi. Res., 2, article 17.
85. L. Eastman, et al., "Undoped AlGaN/GaN HEMTs for Microwave Power Amplification," IEEE Trans. Electron. Devices, 48, p. 479, 2001.
86. Y. Wu, et al., "Very-High Power Density AlGaN/GaN HEMTs," IEEE Trans. Electron Devices, 48, p. 586, 2001.
87. H. Dwight, *Tables of Integrals and other Mathematical Data*, Macmillan, 1961.

REPORT DOCUMENTATION PAGE

Form Approved
OMB No. 0704-0188

1. AGENCY USE ONLY (*Leave blank*)	2. REPORT DATE	3. REPORT TYPE AND DATES COVERED
	February 2003	Technical Memorandum

4. TITLE AND SUBTITLE

Basic Equations for the Modeling of Gallium Nitride (GaN) High Electron Mobility Transistors (HEMTs)

5. FUNDING NUMBERS

WBS–22–755–12–27

6. AUTHOR(S)

Jon C. Freeman

7. PERFORMING ORGANIZATION NAME(S) AND ADDRESS(ES)

National Aeronautics and Space Administration
John H. Glenn Research Center at Lewis Field
Cleveland, Ohio 44135–3191

8. PERFORMING ORGANIZATION REPORT NUMBER

E–13653

9. SPONSORING/MONITORING AGENCY NAME(S) AND ADDRESS(ES)

National Aeronautics and Space Administration
Washington, DC 20546–0001

10. SPONSORING/MONITORING AGENCY REPORT NUMBER

NASA TM—2003-211983

11. SUPPLEMENTARY NOTES

Responsible person, Jon C. Freeman, organization code 5620, 216–433–3380.

12a. DISTRIBUTION/AVAILABILITY STATEMENT

Unclassified - Unlimited
Subject Categories: 33, 76 and 31 Distribution: Nonstandard

Available electronically at http://gltrs.grc.nasa.gov

This publication is available from the NASA Center for AeroSpace Information, 301–621–0390.

12b. DISTRIBUTION CODE

13. ABSTRACT ***(Maximum 200 words)***

Gallium nitride (GaN) is a most promising wide band-gap semiconductor for use in high-power microwave devices. It has functioned at 320 °C, and higher values are well within theoretical limits. By combining four devices, 20 W has been developed at X-band. GaN High Electron Mobility Transistors (HEMTs) are unique in that the two-dimensional electron gas (2DEG) is supported not by intentional doping, but instead by polarization charge developed at the interface between the bulk GaN region and the AlGaN epitaxial layer. The polarization charge is composed of two parts: spontaneous and piezoelectric. This behavior is unlike other semiconductors, and for that reason, no commercially available modeling software exists. The theme of this document is to develop a self-consistent approach to developing the pertinent equations to be solved. A Space Act Agreement, "Effects in AlGaN/GaN HEMT Semiconductors" with Silvaco Data Systems to implement this approach into their existing software for III-V semiconductors, is in place (summer of 2002).

14. SUBJECT TERMS	15. NUMBER OF PAGES
Semiconductor devices; FETs	71
	16. PRICE CODE

17. SECURITY CLASSIFICATION OF REPORT	18. SECURITY CLASSIFICATION OF THIS PAGE	19. SECURITY CLASSIFICATION OF ABSTRACT	20. LIMITATION OF ABSTRACT
Unclassified	Unclassified	Unclassified	